UCLouvain

École polytechnique de Louvain

Low stress interface shear box testing for assessing axial pipe-soil resistance

Author: **Guillaume Martin**
Supervisors: **Hadrien Rattez, Jean-François Vanden Berghe**
Readers: **Jean-Christophe Ballard, Nathan Delpierre**
Academic year 2022–2023
Master [120] in Civil Engineering

Abstract

Accurate and reliable assessment of the axial pipe-soil interaction forces is a key factor for the design of on-bottom submarine pipelines, especially for deep water pipelines as they are operated under high pressure and high temperature and are susceptible to large end expansion, axial walking and lateral buckling.

A key input to assess the axial pipe-soil resistance is the interface strength between the seabed soil and the pipeline coating. This can be measured in the laboratory but standard direct shear testing apparatus needs to be modified to accurately measure the shear strength at the very low stress level existing between the pipeline and the seabed (i.e. typically in the range 5 to 15 kPa).

The modification of the direct shear testing apparatus implies the ability to run interface-soil tests and limitation of the residual stress caused by the friction of the apparatus. The testing procedure then needs to be adapted to realise loop tests with the soil sample.

The purpose of the study is to modify a direct shear test apparatus to perform interface-soil tests in the laboratory to investigate the effect of the pipeline coating roughness, shearing velocity, normal stresses, etc., with the view to compare it with already existing datasets, populate a database of results and develop correlations with soil index parameters.

Some conclusions can then be drawn from this study, such as the usefulness of these tests compared with theoretical values, the usefulness of carrying out low-stress tests and the accuracy of the modified device.

Acknowledgements

I would like to express my gratitude to the individuals and institutions who have supported me throughout the journey of completing this master's thesis.

First and foremost, I would like to thank my thesis supervisors, Hadrien Rattez and Jean-François Vanden Berghe, for their guidance, feedbacks and constant encouragement. Their expertise and dedication played a pivotal role in shaping the direction of this research.

I also thank Jean-Christophe Ballard and Damien Christiaens for their valuable insights and suggestions, which significantly enhanced the quality of this work.

Furthermore, I extend my gratitude to Boris Manette and the members of Fugro's laboratory for their assistance and technical support that proved indispensable in the completion of this thesis.

Finally, as this thesis marks the end of my academic career, my sincere appreciation goes to my family and friends who provided advices and moral support that kept me motivated during the challenging phases of this thesis and my years studying at UCLouvain.

Contents

1 Introduction **1**

2 Description of the initial shear box apparatus **5**
2.1 Initial apparatus 5

3 Direct shear procedure and its modifications to run soil-interface and push-pull loop tests **7**
3.1 Soil-soil direct shear procedure 7
3.1.1 Scope 7
3.1.2 Apparatus 8
3.1.3 Test method 8
3.2 Soil-interface direct shear procedure 10
3.2.1 Scope 10
3.2.2 Differences with the soil-soil procedure 10
3.3 Static push-pull loops shear procedure 11
3.3.1 Scope 11
3.3.2 Software setup 11

4 Shear box modifications and reduction of the residual stress **14**
4.1 State of the art 14
4.2 Initial components 15
4.3 Analysis of residual stress 17
4.3.1 Steel-steel interface 17
4.3.2 Teflon-steel interface 18
4.3.3 Teflon-Teflon interface 19
4.3.4 Teflon-Teflon loop tests 21
4.4 Analysis of the impact of the weight of the upper shear box on the residual stress 23
4.4.1 Experimental friction coefficient 23
4.4.2 Residual stress with additional weight on the shear box . . . 24
4.5 Conclusions 27

5 Characterisation of the sand and the interface **28**
5.1 Particle size distribution (PSD) of the sand . . . 28
5.1.1 Scope . . . 28
5.1.2 PSD curve . . . 28
5.1.3 Hydraulic conductivity . . . 29
5.2 Maximal and minimal density test . . . 30
5.2.1 Scope . . . 30
5.2.2 Results . . . 30
5.3 Normal Proctor test . . . 30
5.3.1 Scope . . . 30
5.3.2 Results . . . 31
5.4 Steel interface . . . 31
5.4.1 Roughness test . . . 32
5.4.2 Link with the normalised roughness . . . 33

6 Assessment of axial pipe-soil resistance **35**
6.1 State of the art and existing datasets . . . 35
6.1.1 Low normal stress . . . 36
6.1.2 Sand density . . . 37
6.1.3 Effect of long displacements . . . 37
6.2 Mass on sample . . . 38
6.3 Effect of soil density and normal stress . . . 39
6.3.1 Tests . . . 39
6.3.2 Comparison with theory and existing dataset . . . 43
6.3.3 Comparison with datasets of different average roughness . . . 45
6.4 50 kPa normal stress test . . . 46
6.5 Effect of large displacements . . . 47
6.6 Confirmation of drained conditions . . . 48
6.7 Imperfections during the tests . . . 49
6.7.1 Decentering during the tests . . . 50

7 Conclusion **53**

A Direct shear procedure Fugro **56**

B Characterisation of the sand **64**
B.1 Particle size distribution (PSD) of the sand . . . 64
B.1.1 Apparatus . . . 64
B.1.2 Test method . . . 64
B.1.3 Result table . . . 65
B.2 Maximal and minimal density test . . . 65

B.2.1 Apparatus 65
B.2.2 Test requirements 66
B.2.3 Test Method 66
B.2.4 Calculations 68
B.3 Normal Proctor test 69
B.3.1 Apparatus 69
B.3.2 Test method 69
B.3.3 Calculations 70

C Roughness graphs of the steel plate **73**

D Assessment of axial pipe-soil resistance **74**
D.1 Effect of soil density and normal stress 74

E Reverse direction tests **76**

List of Figures

1.1 Pipeline-seabed and pipeline-infrastructure interactions [1] 2
1.2 Soil-interface shear resistance as a function of the axial stress [2] . . 3
1.3 Factors affecting axial pipe-soil resistance [3] 4

2.1 ShearSCAN Pro Motorised System [4] 5
2.2 Cylindrical $\varnothing 60mm$ shear box [5] 5
2.3 Scheme of a soil-soil direct shear [6] 6

3.1 Creation of the test in Clisp Studio 12
3.2 Selection of the shear test in Clisp Studio 12
3.3 Selection of the static push-pull loops test in Clisp Studio 12
3.4 Assistant wizard in Clisp Studio 13
3.5 Hardware setup in Clisp Studio 13
3.6 Static push-pull loops consolidation in Clisp Studio 13
3.7 Static push-pull loops shear in Clisp Studio 13

4.1 Scheme of the interface test setup [7] 15
4.2 Lower part of the interface shear box 16
4.3 Steel plate to simulate the pipeline's interface 16
4.4 Upper part of the interface shear box 16
4.5 Interface shearing system assembled 17
4.6 Residual stress with a steel-steel interface between the lower and upper parts of the shear box 18
4.7 Residual stress with a Teflon-steel interface between the lower and upper parts of the shear box 19
4.8 Lower part of the interface shear box with Teflon sheets installed . . 20
4.9 Upper part of the interface shear box with Teflon sheets installed . 20
4.10 Comparison between the Teflon-steel interface and Teflon-Teflon interface 20
4.11 Residual stress with a Teflon-Teflon interface between the lower and upper parts of the shear box. 21
4.12 Residual stress of the shear box during 2 loops 22

4.13 Residual stress of the shear box during 1 loop 22
4.14 Residual stress of the normal shear box and the shear box with added loads on it (1 loop) 26
4.15 Residual stress of the normal shear box and the shear box with added loads on it (2 loops) 26

5.1 PSD curve of the sand 29
5.2 Proctor curve of the white sand 32
5.3 Representation of the five biggest discrepancies between peaks and valleys across a surface to find R_z [8] 33
5.4 Steel plate before the experiments 33
5.5 Steel plate after the experiments 33

6.1 Model for axial resistance [9] 36
6.2 Soil-interface shear resistance as a function of the axial stress [2] . . 37
6.3 (a) Peak and residual shear strength for a sandy specimen at dense and loose state, (b) Volume change during shear for the dense and loose sand [6] 38
6.4 Comparison of the shear stress with 5kPa axial stress between min and max density 40
6.5 Comparison of the shear stress with 10kPa axial stress between min and max density 40
6.6 Comparison of the shear stress with 20kPa axial stress between min and max density 40
6.7 Volume change for maximum and minimum density with a normal stress of 5 kPa 42
6.8 Volume change for maximum and minimum density with a normal stress of 10 kPa 42
6.9 Volume change for maximum and minimum density with a normal stress of 20 kPa 42
6.10 Mean shear stress as a function of the axial stress 42
6.11 Drained friction coefficient as a function of the axial stress 42
6.12 Interpolation of the shear stress at minimum density as a function of the axial stress 44
6.13 Interpolation of the shear stress at maximum density as a function of the axial stress 44
6.14 Dataset of residual stress for silicate sand at low normal stress [10] . 44
6.15 Dataset of silicate sands comparing friction coefficient as function of the normalised roughness [10] 45
6.16 Dataset of silicate sands comparing friction coefficient as function of the normalised roughness [10] 45

6.17 Shear stress 50 kPa max density 46
6.18 Mean shear stress as a function of the axial stress at maximum density 47
6.19 Evolution of drained friction coefficient as a function of the axial stress 47
6.20 2 loops 5 kPa normal stress 48
6.21 2 loops 14,1 kPa normal stress 48
6.22 Comparison of the shearing speed at 20 kPa 49
6.23 Visible imperfections on shear stress vs displacement graphs 49
6.24 Decentering as a function of the initial axial force displayed 51
6.25 Decentering as a function of the initial shear force displayed 51
6.26 Decentering as a function of the applied axial stress 52

B.1 Proctor mould.[11] 67
B.2 CBR mould[12] 70
B.3 Compaction Tamper [13] 71
B.4 Drop pattern for compaction in a CBR mould.[14] 72

C.1 First roughness test 73
C.2 Second roughness test 73
C.3 Third roughness test 73
C.4 Fourth roughness test 73

D.1 Shear stress 5 kPa min density 75
D.2 Shear stress 5 kPa max density 75
D.3 Shear stress 10 kPa min density 75
D.4 Shear stress 10 kPa max density 75
D.5 Shear stress 20 kPa min density 75
D.6 Shear stress 20 kPa max density 75

E.1 Test 10 kPa reverse direction 76
E.2 Test 20 kPa reverse direction 77
E.3 Test 50 kPa reverse direction 77

List of Tables

4.1 Residual stress during loops 23
4.2 Experimental friction coefficients of the steel-steel, Teflon-steel and Teflon-Teflon interfaces 24
4.3 Comparison of the residual mean stress between the normal shear box and the shear box with added loads on it 25

5.1 Diameter of the grain passing the percentiles 29
5.2 Minimum and maximum density. 30
5.3 Dry density of the soil during the normal Proctor test 31

6.1 Mean shear stress of sections of the sand 41
6.2 Mean stress, corrected mean stress and percentage of correction of the sand loop tests 41
6.3 Dynamic friction coefficient of the sand for each pressure and density 43
6.4 Mean shear stress of the sand at max density with 50 kPa of axial stress 46
6.5 Mean shear stress of each loop during 2 loops tests 48
6.6 Shift of each loop 50

B.1 Percentage of grains passing through the sieves after the sieving . . 66
B.2 Dimensions of the mould. 67
B.3 Mass of the minimum and maximum density tests. 68
B.4 Dimensions of the CBR mould. 69

Chapter 1

Introduction

Sub-sea pipelines have emerged as a critical component of modern civilization, facilitating the efficient and reliable transportation of valuable resources across vast distances beneath the ocean's surface. It is "the fastest, safest and most economical and reliable means of transporting oil and gas continuously". [15] As the world's energy demands continue to rise (especially in the Asia Pacific region) and natural resources are discovered in offshore regions, the utilization of submarine pipelines has become increasingly prevalent in the oil and gas industry. This market was evaluated to 13.74 billion US$ and is expected to grow by an average of 7% avery year during the next five years. The figure 1.1 shows the different uses of submarine pipelines interacting with the seabed. [16],[17],[18]

In this context, optimising pipeline design is of the utmost importance as it can result in a good efficiency, a good reliability and service life, low construction and service costs,... The pipeline's design is governed by several factors such as the fluid transported, the heat and pressure in the pipeline and the piping placement. An important factor of pipeline's design is the interaction between the pipeline and the seabed as the pipeline moves on the seabed due to the high pressures and temperatures it operates under. It can significantly affect the structural behavior and integrity of the pipeline during installation and use. The pipeline can be subjected to axial movement, axial walking and lateral buckling. This thesis will mainly focus on the analysis of the axial pipe-soil resistance by runnning laboratory tests with a modified shear box. [19], [20], [21]

The low stress shear box is a laboratory test to assess the axial pipe-soil reaction. The apparatus typically consists of two halves where the soil sample is placed in one half and the interface material is placed in the other half. A shear force is then applied to the lower part, sliding under the other half in the conditions that might be experienced in real-world scenarios. It's complementary with in-situ

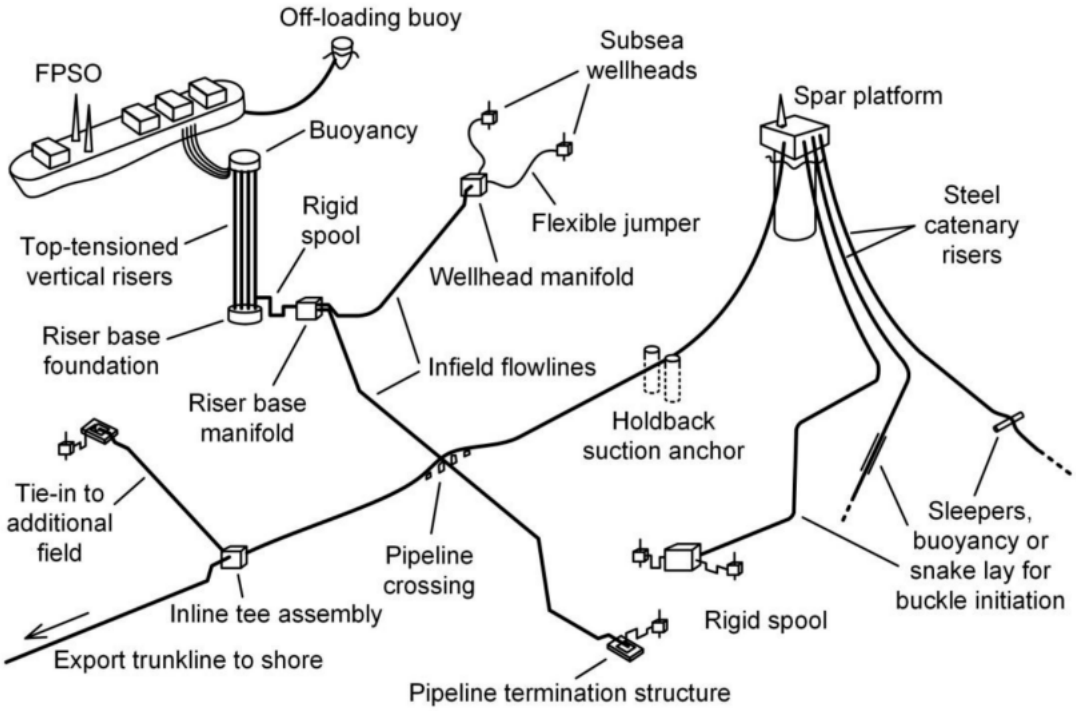


Figure 1.1: Pipeline-seabed and pipeline-infrastructure interactions [1]

and onshore model testing. This test has a lot of advantages, such as the variable velocity, its repeatability, its short duration and low cost to run. It has a simple mechanism and the results can be easely interpreted. It can provide data in drained and undrained conditions, but the drainage conditions are usualyy not very well controlled.
It is a proven concept, but recently used to run tests for pipeline design. The residual friction needs to be minimised. [3]

The typical normal stress created by the pipelines is very low, usually between 2 and 20 kPa, which creates a higher friction coefficient between the soil and the interface compared to higher pressures. We can see on figure 1.2 that at low stress the ratio between shear and axial stress is higher when a low axial stress is applied. This ratio is, by definition, the friction coefficient. The values obtained at higher pressures don't apply to these low pressures, making the tests necessary. In order to test effectively the soil with the least residual stress possible, a modified shear box appparatus has been used. [10]

The experiments were carried out on a direct shear box belonging to Fugro, in their

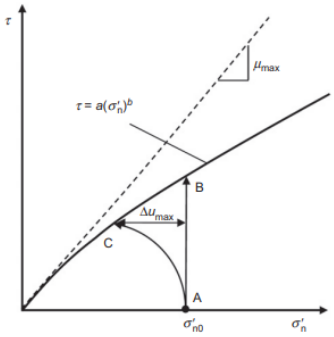


Figure 1.2: Soil-interface shear resistance as a function of the axial stress [2]

laboratory in Louvain-la-Neuve (Belgium). Fugro is a Dutch multinational company that specializes in providing geotechnical surveys and geoscience services to various industries, including offshore energy, construction, infrastructure development, and environmental projects.

The testing apparatus is a usual shear box apparatus normally used to run direct soil-soil tests with 3 majors modifications. First of all, the shear box in itself has been modified in order to run soil interface tests instead of the usual soil-soil tests. Then the shearing procedure has been adapted as the direct shear tests only shears in one direction and we wanted to be able to shear forward and backwards to simulate long displacements. Finally, as the tests are operated under a low normal stress, the residual stress coming from the friction between both parts of the shear box has been reducted as much as possible to limit the interferences on the results of the tests. Different tests had to be run to apply these modifications.

There are several factors controlling the axial pipe-soil resistance. We can name the interface roughness, the normal stress applied, the drainage of the system and a wedging factor. This wedging factor is depending on the embedment of the pipeline: the round shape of the pipeline creates more resistance as the pipeline sinks into the ground. The effect of the normal stress will be given a particular attention in this thesis. We can see them on figure 1.3 and the theoretical representation of these factors.

The tests are all run in drained conditions and the wedging factor is not studied in this document. The studied interface is made out of steel and the soil is a white silicate sand. The roughness of the interface and the different soil index parameters have been tested to classsify them as best as possible. Some other parameters have also been tested such as the sand density and the effect of long displacements.

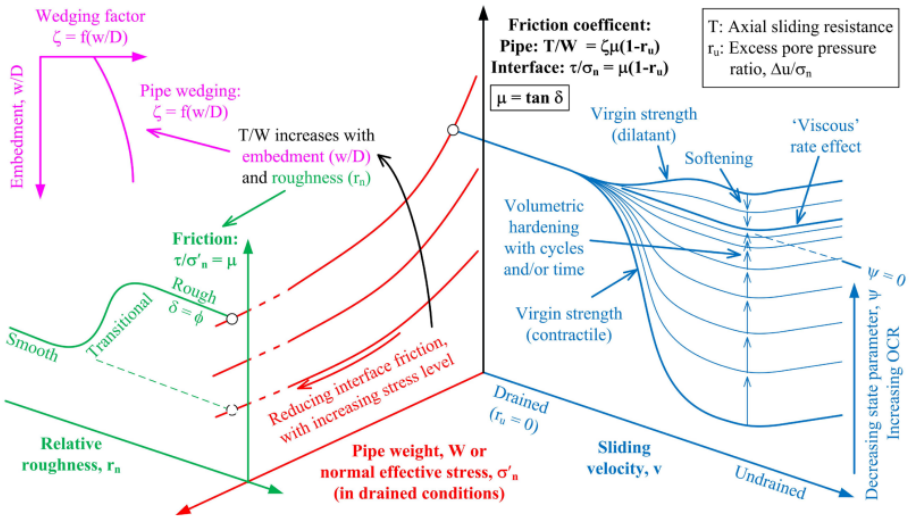


Figure 1.3: Factors affecting axial pipe-soil resistance [3]

Finally, the results have been analysed and put into comparison with the theoretical results and previous studies and the importance of the tests and the error that can be expected in comparison with the theory was dicussed.

Chapter 2

Description of the initial shear box apparatus

In this chapter, the initial apparatus, its components and its mechanism are presented.

2.1 Initial apparatus

The tests performed in this thesis were using a modified normal shear box apparatus made to carry out direct shear tests on soil samples. The apparatus is a ShearSCAN Pro Motorised System from VJTech.

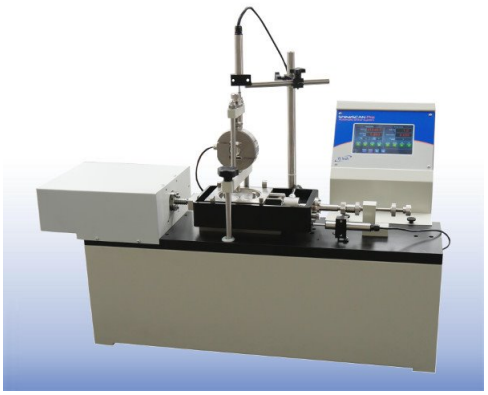


Figure 2.1: ShearSCAN Pro Motorised System [4]



Figure 2.2: Cylindrical $\varnothing 60mm$ shear box [5]

The setup is composed of motors applying vertical and horizontal loads on the

sample with a 3kN load cell measuring the normal force applied, a 1kN submersible load cell measuring the shear force applied in the sample and displacement transducers measuring the horizontal and vertical displacement. In our case, the sample is placed inside a cylindrical shear box, which has a diameter of 60mm. [4][5]

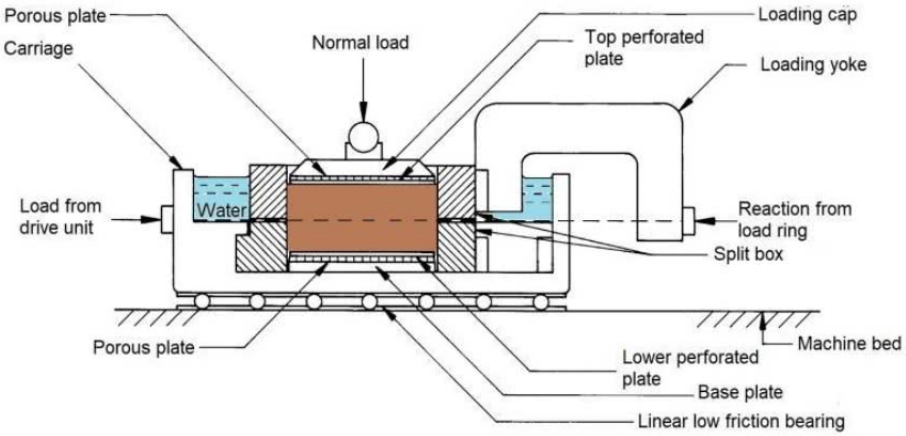


Figure 1 Typical setup for a direct shear test (Head and Epps, 2011)

Figure 2.3: Scheme of a soil-soil direct shear [6]

The load cells have a 1% uncertainty when working over 10% of their maximum capacity and a 5% uncertainty when working between 1% and 10% of their maximum capacity. There is no data available when working lower than 1%.

The shear box is placed inside a carriage and the sample is placed between 2 perforated plates and 2 porous stones with a loading cap placed on top. The figure 2.3 shows a scheme of all the components.

The normal stress applied for direct shear tests can vary from 50 kPa to more than 250 kPa for sands, but this value can vary a lot depending on the soil. This range is well over the one we are going to study (max 20 kPa).

Chapter 3

Direct shear procedure and its modifications to run soil-interface and push-pull loop tests

In this thesis, different types of tests were performed depending on the objective of the test. We can mention empty direct shear tests with an interface-soil shear box, empty push-pull loops tests with an interface-soil shear box, interface-soil direct shear tests and interface-soil push-pull loops tests. As the usual testing procedure for this machine was made for direct shear soil-soil tests, it had to be adapted for the different cases presented previously.
This chapter will present the usual soil-soil direct shear procedure and the needed variations to realise soil-interface tests and push-pull loops tests.

3.1 Soil-soil direct shear procedure

This soil-soil direct shear procedure is the summary of the procedure of Fugro in appendix A. [22]

3.1.1 Scope

The test uses a small (60x60mm square or 60mm $\varnothing$) direct shear box device to measure the shear angle (angle of friction). This is accomplished by moving one side of the box along the other while applying a normal load and horizontal shearing force.
The direct shear box test comprises determining the soil's shear strength parameters (cohesion (c) and friction angle (ϕ)) as well as assessing the soil's stress-strain relationship during shearing.

3.1.2 Apparatus

- SSP: Shear Scan Pro – shear box apparatus
- Digital Calliper
- Shear box moulds
- A steel cylinder and dead blow hammers for the compaction
- Plastic water disposer
- Water content tins
- Calculator
- Scale
- Oven

3.1.3 Test method

Sample preparation

The soil used for the test is run through a 2.0 mm sieve. The 2-4mm particles are checked and must pass through a 4mm sieve if any particle larger than 2mm is present. Larger particles can be crushed so they can pass through a sieve with a 4mm opening. It is important to note if particles are retained on the 2mm sieve.

First, the moisture content is adjusted by weighing the sample and adding the required water mass to meet the wet density mass. The dry density can then be multiplied by the water content to determine the bulk density. We then calculate the required mass for the test by multiplying the volume of the mould you intend to use by the bulk density. Sample height needs to be around 22mm. Utilizing the digital calliper, the diameter is measured. Weigh and record the top cap, porous stone, and metal plate (mass on sample). We place the bottom disc first, followed by the porous disc and the porous stone, and then weigh the finished shear box.

Compaction

The required sample mass is divided into three equal sub samples in three separate bags. The first portion is added into the shear box, then the steel cylinder is put over the portion and the sub sample is compacted by striking the cylinder with the hammer. The height is then measured using a digital calliper. An unequal surface is created in between layers and this step is repeated with the next two portions.

Each layer is measured until the final layer is about 22mm, each layer should be about the same heigth. The sample is weighed to verify that the bulk density is within 2 percents of the calculated dry density.

Software setup

Using the Clisp Studio software, we can create the Client, Job file number, Borehole number, Sample number and the test name.
Then we select the number of phases that will be run in the Assistant wizard and open the hardware setup to select which machine we will be running. These parameters are copied across all the specimens.
In the specimen details, the consolidation and shear stage parameters are set. Then we enter the datas of the test that will be run.

Consolidation stage

The porous stone, porous disc and top cap are placed on the shear box before inserting it into the machine. We have to press the "engage" button after setting up the loadcell and displacement transducer to apply a seated load. The square root times table is used to hold the consolidation data and the stop conditions are specified for 18 minutes. If doing clay samples, this will need to be changed because the consolidation and shearing periods will be greater. The start time, beginning vertical load and displacement are recorded once the consolidation's settings have been established and before pressing the "run" button. The sample needs to be immersed in water from the jug at this point because the stress will be imposed instantly. Tap water is used. Finally, the end time, vertical load, vertical displacement of the sample and the t100 value are recorded.

Shear stage

The box is connected to the load cell on the horizontal surface while maintaining the normal pressure on the sample. If we apply low vertical stress, the initial horizontal stress shown on the screen should be less than 10N and positive. To ensure that the horizontal bar may move freely at all times, the nut needs to be manually tightened and then turned back a little less than a quarter of a turn. Driving the other screws down until there is a small gap between the boxes (this should not exceed 1mm) and then backing them off so they are not touching the lower box will unlock the two halves of the shear box. Clisp warns us before shearing begins. The vertical and horizontal loads and the displacements are then recorded.

Unloading the sample

Once the shearing and reverse stages are finished, we drain the water from the carriage by the tap on the carriage, unload the loadcells and disconnect them. The sample is removed and put in a tin which is then placed in the 107°C oven for 16 hours to take a final water content.

The machine should be cleaned at the end of each stage.

3.2 Soil-interface direct shear procedure

These tests were carried on to analyse the residual stress of the shear box without a sample, in order to reduce it.
The procedure is similar to the soil-soil procedure but with some difference due to the replacement of the lower part of the shear box to fit the desired interface.

3.2.1 Scope

The test aims to determine the shear strength properties of a soil sample on a defined interface using a 60mm ø shear box apparatus under controlled shear stress conditions. This is achieved by one half of the box, containing the tested soil, sliding along another, containing the tested interface, with a normal load and horizontal shearing force applied.
The scope of the soil-interface direct shear box test can include the determination of the shear strength parameters of the soil on the interface and the evaluation of the stress-strain relationship of the soil during the shearing.

3.2.2 Differences with the soil-soil procedure

The only differences with the the soil-soil procedure are the shear box moulds, the sample preparation and the compaction of the sample.

As the shear box moulds have to fit an interface, the lower and upper parts of the regular shear box are replaced by a lower part fitting the interface; the upper part is also replaced to fit the lower part and to be able to be connected with the lower part. The diameter of the shear box remains unchanged. The interface-soil mould can be seen on figure 4.5.

The soil sample is only present in the upper part of the shear box. It was decided to keep a sample heigth of eleven cm as it corresponds to the heigth of sample in the upper part of the shear box during soil-soil tests. The mass needed for this

test is then two times smaller than the soil-soil direct shear.

The sample doesn't need to be devided in three parts anymore, as the sheared soil is located at the bottom of the sample. The sample can be put at once but still needs to be compacted by striking the steel cylinder with the hammer and the sample should be measured with the digital calliper to make sure its heigth is equal to 11 cm.

3.3 Static push-pull loops shear procedure

These tests were carried out to test the samples during large displacements. All the tests run to analyse the soil-interface shear strength were static push-pull loops.

The static push-pull procedure is similar to the direct shear procedure but with a few changes regarding the software setup, Clisp Studio, that will be explained here under.
The other steps can be found in sections 3.1 and 3.2.

3.3.1 Scope

The test aims to determine the shear strength properties of a soil sample using a modified 60mm ∅ shear box apparatus under controlled stress conditions. This is achieved by one half of the box sliding along another with a normal load and horizontal shearing force applied.
In our case, the aim of the push-pull loops test is make a soil-interface test, the lower part of the shear box has been replaced by a new part that can fit an interface. The scope of this test includes the evaluation of the stress-strain relationship of the soil during the shearing, especially ragarding long displacements.

3.3.2 Software setup

Here are the steps and illustrations on how to realise a cyclic push pull test on Clisp Studio:

1. We create a new test by right-clicking on a test already been created for the client or create a new client and a new trial (figure 3.1).

2. We select "Essais de résistance au cisaillement direct, simple, annulaire et dynamique" (figure 3.2).

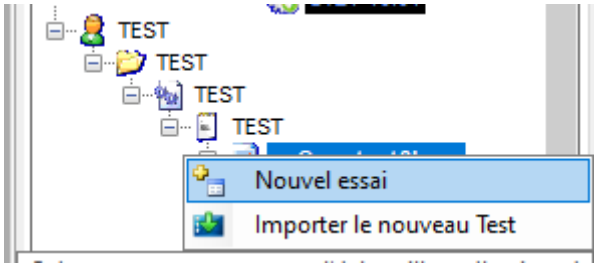


Figure 3.1: Creation of the test in Clisp Studio



Figure 3.2: Selection of the shear test in Clisp Studio

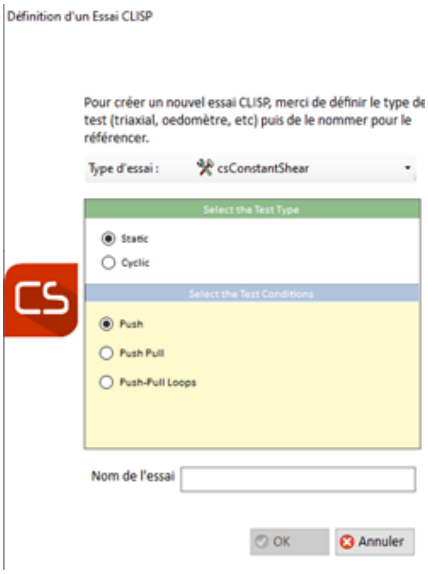


Figure 3.3: Selection of the static push-pull loops test in Clisp Studio

3. We select csConstantShear in “Type d’essai”, Static in "Test type", Push-Pull loops in "Test conditions" and give a name to the test (figure 3.3).

   The test has now been created.

4. We select the Hardware setup in the assistant wizard and make sure the right channel is selected, then enter the specimen details (figures 3.4 and 3.5).

5. We configure the consolidation settings (Single stage, multiple stage or over-consolidation possible) (figure 3.6) .
   We can add stages by clicking on Add and see the theoretical consolidation form in Waveform.

6. We configure the shearing (figure 3.7).

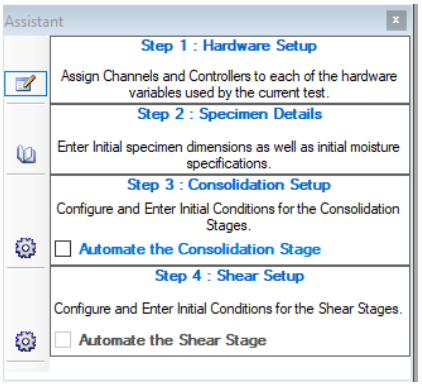


Figure 3.4: Assistant wizard in Clisp Studio



Figure 3.5: Hardware setup in Clisp Studio

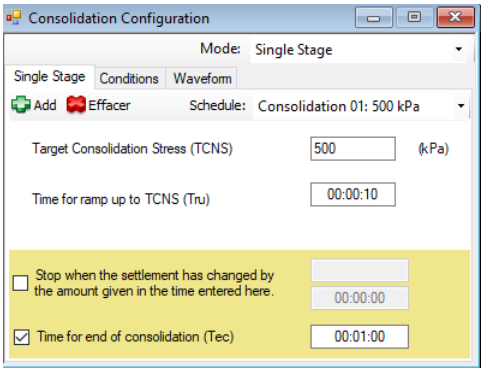


Figure 3.6: Static push-pull loops consolidation in Clisp Studio

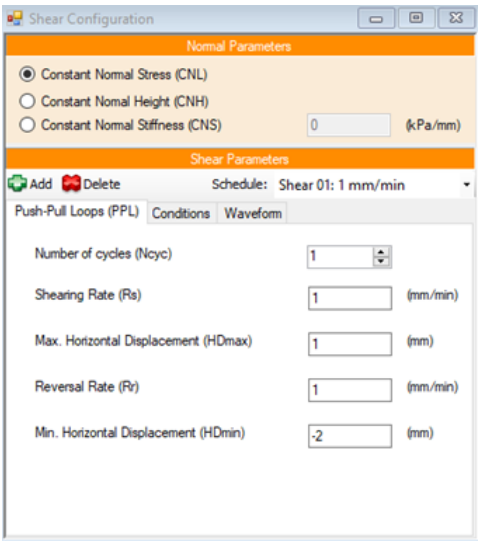


Figure 3.7: Static push-pull loops shear in Clisp Studio

The test is ready to be executed if the shear box set in the apparatus.

Chapter 4

Shear box modifications and reduction of the residual stress

This chapter will present the different modifications of the shear box system to go from a usual soil-soil shear box system to an interface-soil system needed for the tests. Then some tests and modifications to reduce the residual stress will be presented. Finally, these modifications and results will be compared with the existing datas on a similar equipment.

4.1 State of the art

Researches on this subject led to two articles that gave informations about an apparatus to perform interface-soil shear box testing at very low pressures and the modifications that were performed from the original apparatus: White et al, 2017 [2] and Meyer et al, 2015 [7]. Here are the important informations about their respective setup.

The first study used a direct shear box apparatus adapted to perform tests at low stress. This was done by replacing the vertical loading system by a dead-weight load frame. The residual stress was tested by running tests as if it was a usual interface-soil test but without any sample in the shear box. The residual stress caused by the friction between the upper half and the lower half of the shear box was measured at 0,5 kPa. This value is substracted to every test using this setup in order to correct the results.

The second study also used a direct shear apparatus already with a dead-weight load frame. Its modifications include a lightweight top cap and load hanger and the installation of a new low capacity load cell of 120N. The upper part of the

shear box is sliding over an interface block that covered the travel of the shear box in their configuration. The shear box was also modified as PTFE (Teflon) sheets were placed under the top half of the shear box to reduce the friction the shear box and the interface. A scheme of this setup is shown on figure 4.1.

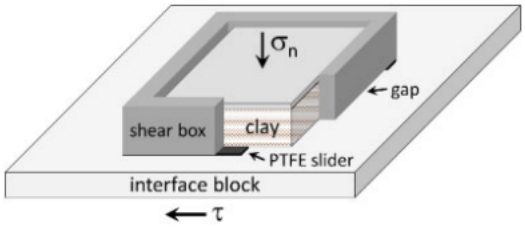


Figure 4.1: Scheme of the interface test setup [7]

Like in the other article, the residual stress was measured by running tests without samples. The frictional load was measured at 2,6N which is equal to a frictional stress of 0,26 kpa (a 100mmx100mm shear box was used). This value was also substracted from their results to correct them.

These setups show some possible modifications that can be implemented on our apparatus and a good target in term of residual frictional stress after modifications.

4.2 Initial components

In order to realise some interface-soil tests, the lower part of the shear box had to be replaced. The new lower part is shown on figure 4.2. It can host a plate of the material we want to test, simulating the interface of a pipeline. The plate tested is a steel plate (shown on figure 4.3).
The replacement of the lower part of the shear box induced a change of the upper part ot the shear box as well, as it was impossible to screw both parts together to prepare the sample. The new upper part has a rectangular shape with a width of 80,22mm, a length of 122,14mm and a heigth of 23,8mm. It has a whole with a diameter of 60mm at its center to host the soil sample. It wheigths 1250 grams This new piece is shown on figure 4.4.
From this point, all the pieces were gathered but had to be put together to create a functionnal system. The first stage was to assemble the shear box and being able to place it into the ShearSCAN system. The hook and blackbox from a normal direct shearbox were compatible in length with the system, but the upper part of the shear box had do be screwed to the left holes of the lower part on the figure 4.2. The measured weight of the upper part of the shear box, black box, hook and

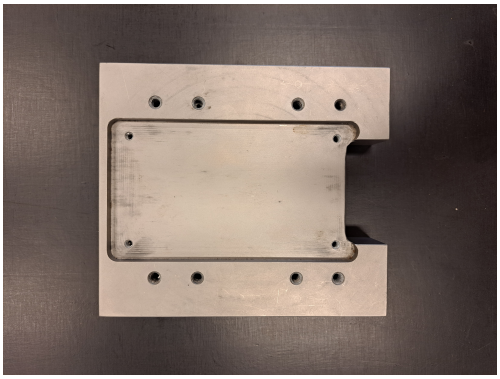


Figure 4.2: Lower part of the interface shear box



Figure 4.3: Steel plate to simulate the pipeline's interface

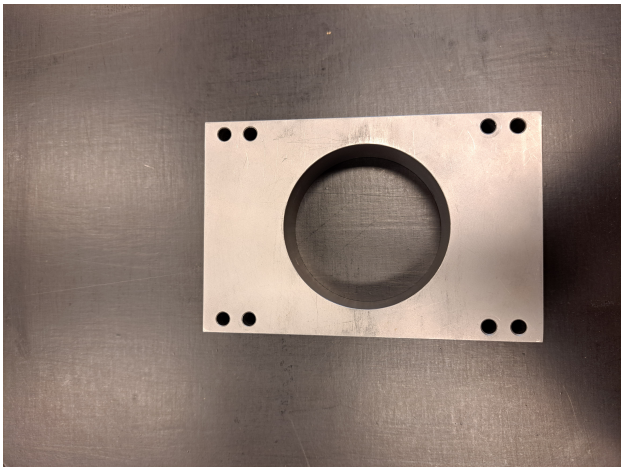


Figure 4.4: Upper part of the interface shear box

screws is 1481 grams.
Then, the steel plate didn't fit perfectly into the lower part of the shear box so that it had room to move. 2 small plastic pieces were used to fill in the gap and fix the plate into the lower part of the shear box.

The figure 4.5 shows how all the previous parts were assembled.

Together, these components weigh 4,4 kg which require a careful manipulation and an adapted capacity balance.

The shear box can be moved forward or backwards in order to adjust its position, so that the axial load and the middle of the sample are perfectly aligned.

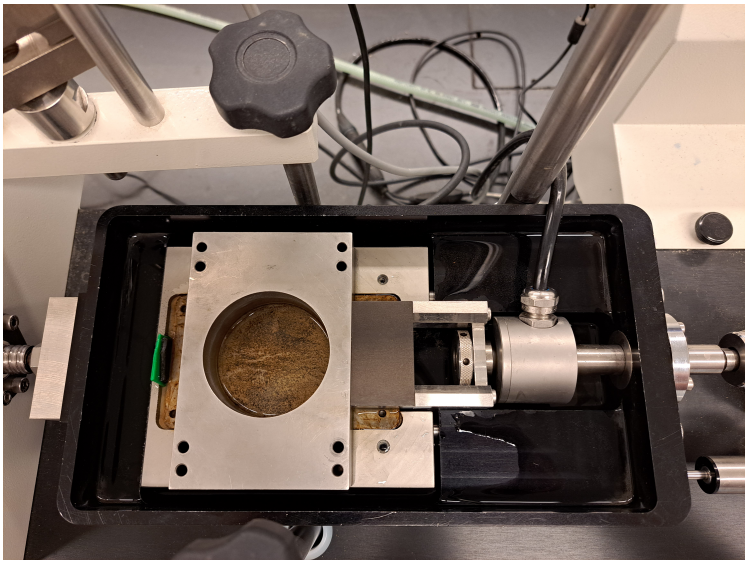


Figure 4.5: Interface shearing system assembled

Some tests were then conducted to assess and reduce the residual shear stress of the system.

4.3 Analysis of residual stress

4.3.1 Steel-steel interface

The tests were conducted by running a direct shear on an empty shear box (in submerged conditions). The shear stress is always calculated by reporting to the area of the shear box (a circle of 60 mm of diameter) because it's easier to substract this value to the shear stress obtained with a sample as they are both based on the same area. The shearing settings were the following: shearing speed of 0,45mm/min and a shearing length of 8% of the shear box diameter: 4,8mm. One test was conducted after performing a push-pull loop on a sand sample between +10mm and -10mm in order to see the difference of the residual stress between the beginning and the end of a sample test. The sand sample was removed from the shear box, but the sand grains stuck between both parts of the shear box were left. The results of the different tests are presented on figure 4.6.
On this figure (figure 4.6), we can see the residual stress of the shear box with a steel-steel interface depending as a function of the displacement. The tests realised with an empty shear box are shown in blue, while the test realised after the shearing of a sand sample is shown in red.

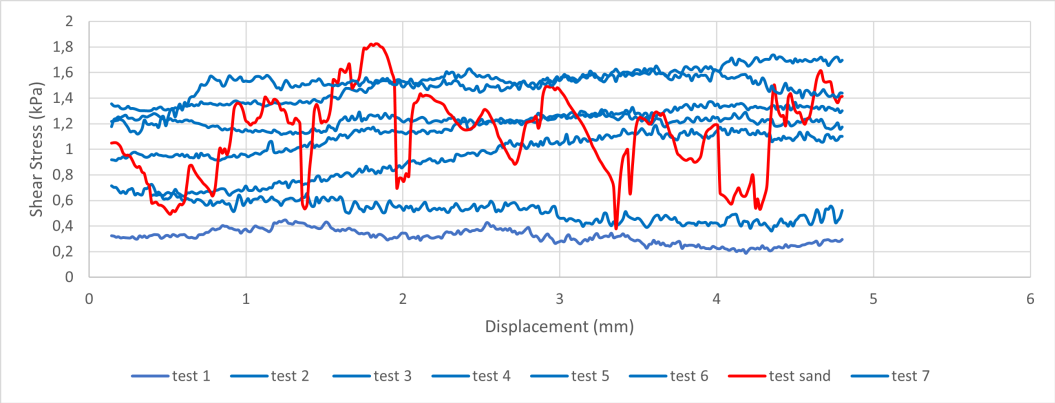


Figure 4.6: Residual stress with a steel-steel interface between the lower and upper parts of the shear box

The mean residual stress before shearing a soil sample is 1,02 kPa (starting after 0,14 mm, the stress rise at the beginning of the test isn't taken into account), while the mean residual stress of the test after shearing a soil sample is 1,12 kPa. We can see that the mean residual stress after the soil sample is, on average, similar to the residual stress before the sample, but it creates a lot of noise during the test. As the mean residual stress of 1,02 kPa is quite high regarding the fact that the sample will be tested at low stress values (beginning at 5 kPa), some attempts were made to reduce the residual stress.
If we consider that the residual stress comes only from the mass of the upper part of the shear box, we can try to reduce it by analysing the components shear force: $F = \mu * N$ where μ is the friction coefficient and N is the normal force (the weight of the upper part of the shear box). The only ways to reduce the residual stress are to reduce the coefficient of friction or to reduce the normal force which, in this case, is the weight of the upper part of the shear box.

4.3.2 Teflon-steel interface

It was then decided to reduce the cfriction coefficient by using Teflon sheets at the interface of the shear box. This is a similar approach to the one of Meyer et al as described in section 4.1.

First, some Teflon sheets (also known as PTFE sheets) were installed on the top of the lower part of the shear box, creating a Teflon-steel interface between both parts of the shear box. The figure 4.8 shows the Teflon installed on the lower part of the shear box. As the Teflon sheets have a non-negligible thickness, the rest of the lower part doesn't touch the upper part of the shear box. The theoretical friction

coefficient between Teflon and steel is 0,1. This value was provided by HPProducts, the Teflon sheets's supplier. To put things into persepctive, the friction coefficient of a wet steel-steel interface is estimated to be between 0,2 and 0,3.
As 2 Teflon sheets of different thicknesses were provided, they were both tested to make sure we would obtain the same values. The first one is a grey sheet with a thickness of 0,29mm and the second one is a brown sheet with a thickness of 0,13mm.
The shearing parameters were the same as the steel-steel interface. The results of the tests are shown on figure 4.7

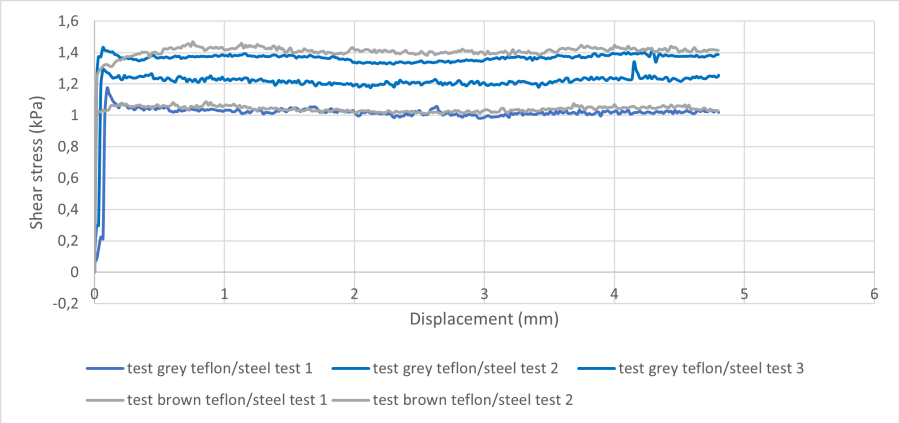


Figure 4.7: Residual stress with a Teflon-steel interface between the lower and upper parts of the shear box

As we can see on the figure 4.7, the 2 different Teflon sheets have a similar friction coefficient, which confirms that their only difference was their thickness. The mean residual stress value for those tests (starting after 0,14mm) is equal to 1,21 kPa. Compared to the 1,02 kPa obtained with a steel-steel interface it's not an improvement, which is quite unexpected regarding the supposed coefficients of friction of both interfaces.

4.3.3 Teflon-Teflon interface

It was then decided to install some Teflon under the upper part of the shear box as well, to create a Teflon-Teflon interface, which has an even lower theoretical coefficient of friction. The theoretical coefficient of friction of a Teflon-Teflon interface is located between 0,04 and 0,1. The pieces of the shear box with the Teflon sheets installed are shown on figures 4.8 and 4.9.
The Teflon sheets were installed such that the shearing interface would only be Teflon-Teflon while doing push-pull loops between +10mm and -10mm.

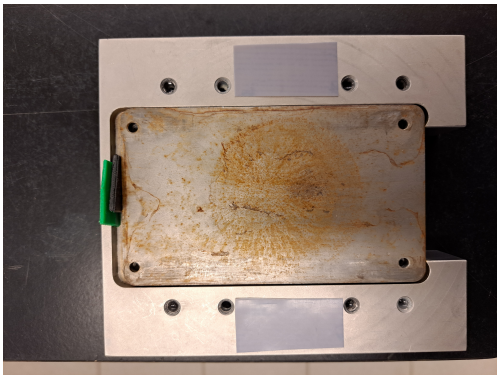


Figure 4.8: Lower part of the interface shear box with Teflon sheets installed

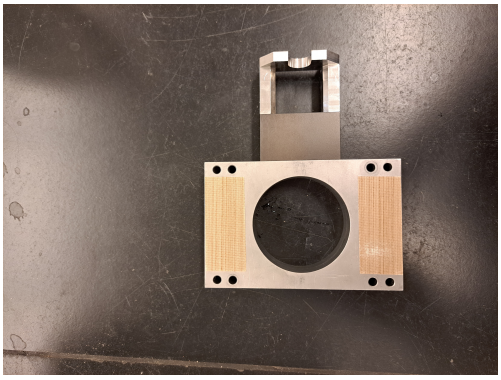


Figure 4.9: Upper part of the interface shear box with Teflon sheets installed

The results of the empty shearing tests are compared to the previous Teflon-steel interface and shown on figure 4.10.

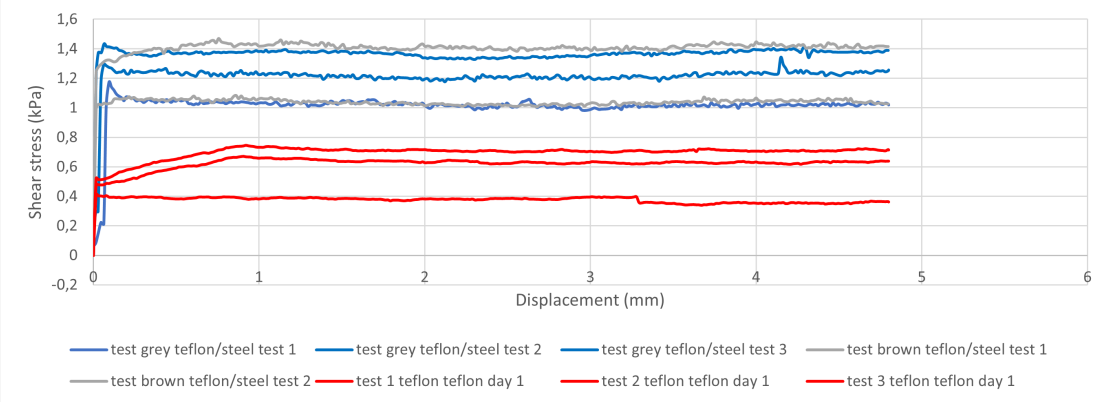


Figure 4.10: Comparison between the Teflon-steel interface and Teflon-Teflon interface

We can clearly see that having a Teflon-Teflon interface reduces the residual stress compared to a Teflon-steel interface. Some other tests were then conducted and the mean residual stress obtained is 0,53 kPa. This is a huge improvement compared to the steel-steel and Teflon-steel interfaces.

Another test to assess the mean residual stress of this interface after a soil sample was carried out, it resulted in a mean residual stress of 0,91 kPa which is an improvement compared to the first one with a steel-steel interface (1,12 kPa). This value is higher than the mean before a soil sample but cannot be reduced much

more. The result of this test put into comparison with the Teflon-Teflon interface tests before a sample can be seen on figure 4.11 .

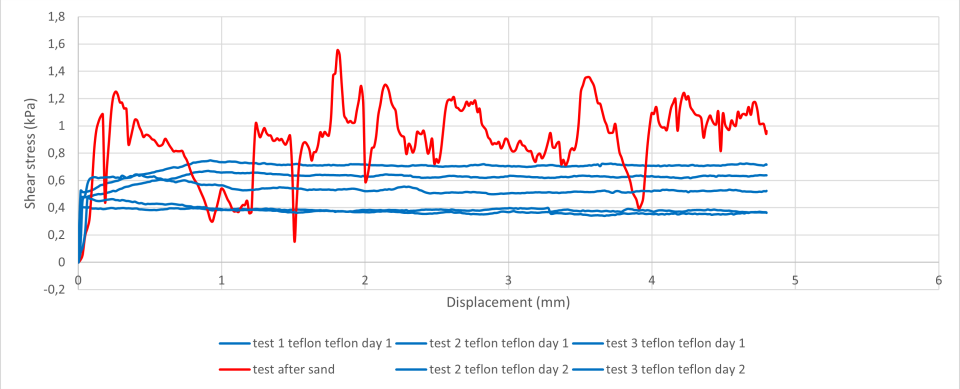


Figure 4.11: Residual stress with a Teflon-Teflon interface between the lower and upper parts of the shear box.

4.3.4 Teflon-Teflon loop tests

The final step of the friction coefficient's reduction was to test the residual stress during a full motion of the shear box. Several tests were run to estimate the average residual stress during a loop test and check its value compared to the previous ones obtained with direct shear tests. It's important to test the residual stress on a whole loop because the samples will be tested on a similar loop. There can be a difference in the residual stress of the shear box going forward or backwards or an effect of the long displacements.

As some values of the test can't be kept in the calculation of the mean residual stress, such as the first rise of shearing and the shifts from forward to backwards motion, it was decided to calculate the mean residual stress by taking the values from 5 to 9mm, 4 to -4mm and -7 to -3mm. The mean of those portions were then calculated and the overall mean of those values gives us the mean residual stress (the mean between 4 to -4mm was taken 2 times as the section is twice longer).

Four tests were run with an empty shear box to assess the mean residual stress: 2 tests with 1 loop each and 2 tests with 2 loops each. We can see the results of the 2 loops tests on figures 4.12 and 4.13. The sections used to calculate the mean stress of the loops are encircled in red on figure 4.12.
We can see for both graphs on this figure that there is a decentering of the results, with the forward motion stress being higher than the backwards motion stress.

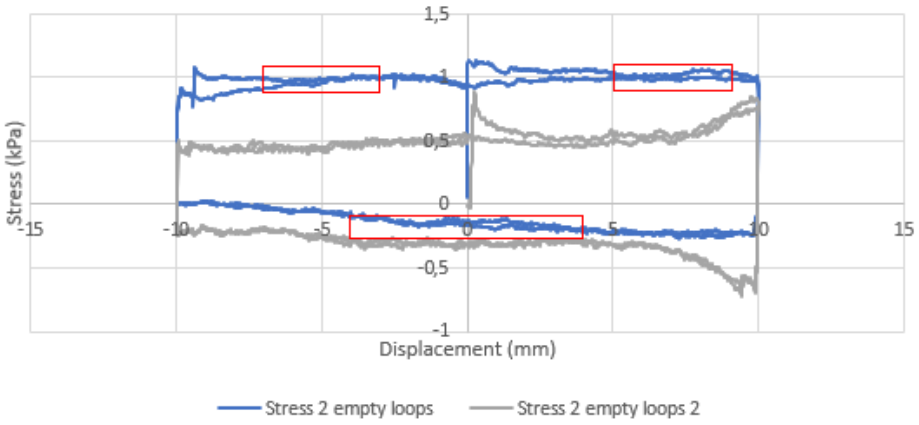


Figure 4.12: Residual stress of the shear box during 2 loops

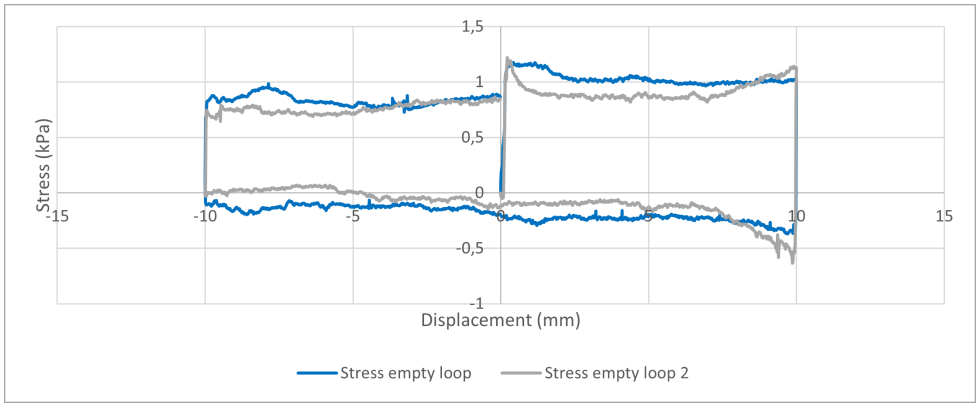


Figure 4.13: Residual stress of the shear box during 1 loop

Furthermore, the graph in grey has 2 peaks, one at the beginning of the loop and another one when the shear box goes from a forward motion to a backwards motion. These phenomenons will be studied later in the document.

The mean residual stress of the different tests and sections of each test are reported in table 4.1.
We can see that the mean value of each loop is in a similar range. The mean residual stress of these loops is 0,49 kPa with variations under 0,1 kPa. Compared to the 0,53 kPa obtained for the direct shear stress, it's very close. We can see that the values of the mean between 5 and 9mm are pretty high due to the decentering.

We are going to substract 0,5 kPa to correct the results obtained with the shearing of sand samples. This correction will give us a good estimation of the real shearing

Test	Mean 5 to 9mm (kPa)	Mean 4 to -4mm (kPa)	Mean -7 to -3mm (kPa)	Total Mean (kPa)
1 loop test 1	0,99	-0,18	0,80	0,54
1 loop test 2	0,90	-0,08	0,74	0,45
2 loops test 1 cycle 1	1,03	-0,14	0,99	0,57
2 loops test 1 cycle 2	0,99	-0,16	0,96	0,57
2 loops test 2 cycle 1	0,58	-0,30	0,47	0,41
2 loops test 2 cycle 2	0,53	-0,31	0,45	0,40

Table 4.1: Residual stress during loops

stress of the sand samples.

4.4 Analysis of the impact of the weight of the upper shear box on the residual stress

During the previous tests, we changed the interface materials to reduce the residual stress. As the Teflon is one of the components with the lowest friction coefficient, we won't try to change it anymore.
The other parameter that we can change is the normal weight, which is the weight of the upper shear box in this case, as explained at the end of the subsection 4.3.1.

4.4.1 Experimental friction coefficient

As the creation of a new lighter upper shear box would have needed a lot of ressources and could have led to other problems, it was decided to test the effect of the weight of the upper shear box, black box and hook on the residual stress by adding some weight on it and see the results. It wasn't sure that the residual stress could be reduced by the weight of the upper part of the shear box because the friction coefficients of the previous interfaces, calculated with the average residual stress and the weight of the upper part of the shear box, are higher than the expected friction coefficient. The hypothesis is that there could be some residual stress coming from the shearing apparatus. The results of the calculations can be seen in table 4.2.
These results show that the friction coefficient is very low for every cases, but the

interface	upper parts weight	residual stress	friction coefficient
steel-steel	1481 g	1,02 kPa	0,20
Teflon-steel	1481 g	1,21 kPa	0,24
Teflon-Teflon	1481 g	0,53 kPa	0,10
Teflon-Teflon loop	1481 g	0,49 kPa	0,096

Table 4.2: Experimental friction coefficients of the steel-steel, Teflon-steel and Teflon-Teflon interfaces

Tefon-steel interface is far off the theoretical value, being more than twice bigger than the expected value. The Teflon-Teflon interface was, on the opposite, very effective. Because of the decentering during the loop tests, it is difficult to check the accuracy of the direct shear results, but the loop tests don't have this problem. With such low friction coefficients, it seems that a lighter upper part of the shear box might be a good way to continue the reduction of the residual stress. To make sure that this would have an impact, it was decided to put more load on the shear box and see if the shear stress would raise.

4.4.2 Residual stress with additional weight on the shear box

As explained in the previous subsection, this experiment was decided because it is easier to add some weight on the shear box than manufacturing a new piece. It's a good way to test if the production of a new lighter upper part of the shear box would be an effective way to reduce the residual stress.

Two different loads were added on the upper part of the shear box. One load plate of 497 grams and the other with 2 plates for a total of 995g. Comparing the density of steel (7850 kg/m^3) and plastic (1240 kg/m^3 for the most used printing plastic filaments [23]), a change of material of the upper part of the shear box could reduce the load by over 1000 grams.

The tests were carried out with both loads performing 1 loop and a test with the 995g load was also performed. The results of the tests are shown on figures 4.14 and 4.15 and compared to the previous results without any added load.
We can see that apart from 1 graph with a load of 1kg doing 1 loop, the results with the loads are in the same range as the unloaded ones. The mean values of each tests are reported in table 4.3.

These results show that the addition of the loads had nearly no impact on the

Test	Mean 5 to 9mm (kPa)	Mean 4 to -4mm (kPa)	Mean -7 to -3mm (kPa)	Total Mean (kPa)
Empty loop 1	0,99	-0,19	0,80	0,54
Empty loop 2	0,90	-0,08	0,74	0,45
1 Loop load 500g	0,95	-0,01	0,87	0,46
1 Loop load 1kg 1	1,50	-0,87	1,12	1,09
1 Loop load 1kg 2	0,55	-0,64	0,53	0,59
2 loops test 1 cycle 1	1,03	-0,14	0,99	0,57
2 loops test 1 cycle 2	0,99	-0,16	0,96	0,57
2 loops test 2 cycle 1	0,58	-0,30	0,47	0,41
2 loops test 2 cycle 2	0,53	-0,31	0,45	0,40
2 loops load 1 kg cycle 1	0,66	-0,47	0,60	0,55
2 loops load 1 kg cycle 2	0,64	-0,45	0,55	0,52

Table 4.3: Comparison of the residual mean stress between the normal shear box and the shear box with added loads on it

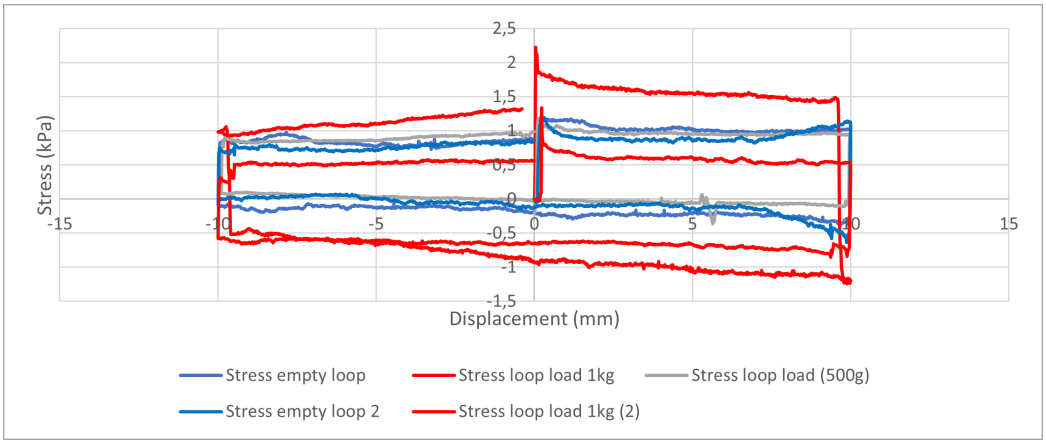


Figure 4.14: Residual stress of the normal shear box and the shear box with added loads on it (1 loop)

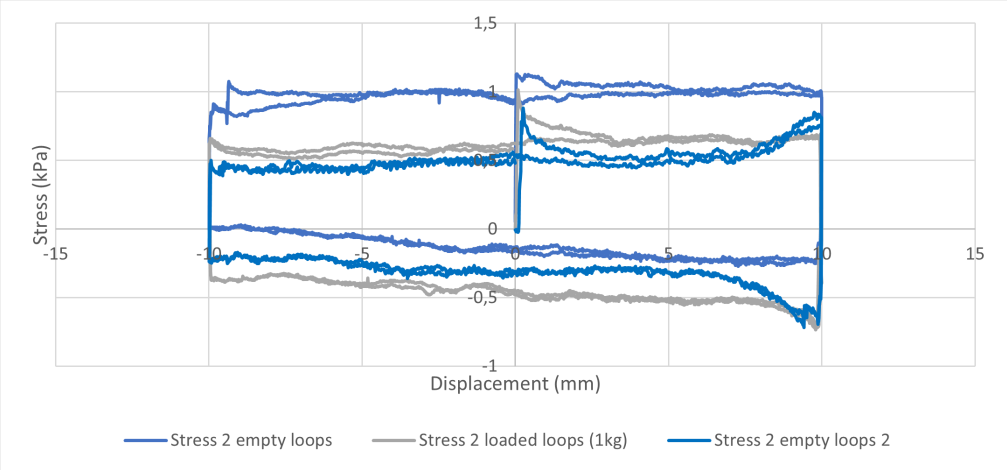


Figure 4.15: Residual stress of the normal shear box and the shear box with added loads on it (2 loops)

results aside from 1 test with a mean of 1,09 kPa. Given its difference with the other tests in the same condition, the hypothesis is that the test wasn't operated correctly and that the increase of stress is due to an external factor and not the loads on it. The 3 other loops with a load of 1 kg show a mean stress of 0.59, 0.55 and 0.52 kPa. The loop with a load of 497 g even showed a mean stress lower than the mean stress without added loads.
The conclusions of this test are that the residual stress is very difficult to reduce even more from this point and that there might be some residual coming from the equipment when the tests are performed.

4.5 Conclusions

The modifications of the shear box resulted in the replacement of the usual shear box by a soil-interface shear box with some plastic pieces to fit the interface plate into its support.

The reduction of the residual stress resulted in the addition of Teflon sheets on both parts of the shear box sliding along another. The average residual stress obtained during a push pull loop between 10 mm and -10 mm is 0,49 kPa, which is similar to the value obtained by White et al, 2017 but about twice bigger than the value obtained by Meyer et al, 2015.
Compared to the modifications stated in the state of the art, the replacement of the shear box and application of Teflon sheets were similar, no changes were made on the load cells and loading systems as it doesn't improve the residual stress but the confidence in the accuracy of the tests. Our results were always in the same range, especially for the loop tests and these modifications would have repercussions beyond the scope of this thesis.

Finally, the impact of the weight of the upper part of the shear box was judged minimal on the final residual stress obtained, so no changes were done on that side.

Chapter 5

Characterisation of the sand and the interface

5.1 Particle size distribution (PSD) of the sand

In order to determine the hydraulic properties of the sand, especially the hydraulic conductivity, the particle size distribution of the soil needs to be known. The particle size curved can be determined by completing a grain size analysis. This test was realised following the instructions of European standards [24][25].

5.1.1 Scope

This test aims to determine the diameter of soil particles between 0,063 and 80mm. The tests consists in separating a soil sample into different diameters by passing it through a serie of sieves and reporting the mass of each sieve. The dimensions of the sieves depend on the soil and the wanted precision.
In our case, as the sand has a low percentage of fines (less than $63\mu m$), a sedimentation test is not necessary. If the soil had more than 10% of fines, it would have been mandatory.

The test method, apparatus and result tables can be found in appendix B.1.

5.1.2 PSD curve

We can then create the PSD curve of the sand using the percentage of grains passing through sieves. The PSD curve is presented on the figure 5.1.

The values of D_{10}, D_{50} and D_{90} are marked with a red dot on the graph and the values are reported in table 5.1.

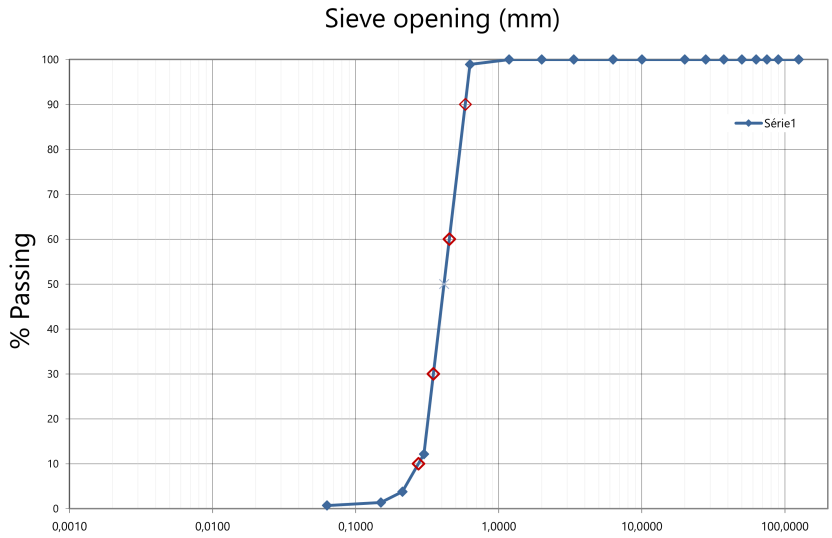


Figure 5.1: PSD curve of the sand

Percentile	D_{10}	D_{50}	D_{90}
Diameter (mm)	0,27	0,41	0,58

Table 5.1: Diameter of the grain passing the percentiles

5.1.3 Hydraulic conductivity

As our tests will be run in drained conditions, it is important to make sure the shearing speed allows to stay in these conditions. The amount of water or other fluid that can pass through the voids of a porous material is a property called permeability or hydraulic conductivity. [26] The determination of the hydraulic conductivity can give us the maximum speed of the water passing through our soil and thus a maximum value for the shearing speed of our tests in order to stay in drained conditions.

A commonly used formula to assess the hydraulic conductivity of sands was proposed by Hazen in 1911 [27]:

$$K = C * D_{10}^2$$

Where K is the hydraulic conductivity in mm/s, C a constant usually taken as 1 and D_{10} the diameter of the 10% percentile of the sand in mm.
In our case, we obtain a conductivity of 0,75 mm/s. We will have to make sure that the shearing speed of our tests is under this value to stay under drained conditions.

The usual direct shear speed for sands (0,45mm/min) can be taken for our tests as it allows drained conditions during the test.

5.2 Maximal and minimal density test

5.2.1 Scope

This test applies to non-cohesive soils. In our experiments, the effect of the density of the soil on the interface-soil shear stress will be tested. To do so, it is interesting to quantify the maximal and minimal density of the dry sand. The test procedure is based on the standard NF P94-059. [28]

The test method, apparatus and calculations can be found in appendix B.2.

5.2.2 Results

The values of the minimum and maximum density are presented in the following table:

Density	Value
$\rho_{d,min}$ (kg/m^3)	1499,6
$\rho_{d,max}$ (kg/m^3)	1665,5

Table 5.2: Minimum and maximum density.

We can see that there is a notable difference between the two values. The effect of the density on the soil/interface shear will be tested further in the present document.

5.3 Normal Proctor test

The test procedure is based on the standard NF P 94-093. [13]

5.3.1 Scope

The Proctor test aims to determine the compacting characteristics of a soil. The test principle consists to humidify a soil sample to different water contents and compact it with a conventionnal procedure and energy. For each of the considered water contents, the dry density of the soil is determined and a variation curve of the dry density as a function of the water content is established.

This curve, called Proctor curve, presents a maximal value of the dry density at a specific water content. Those are two values called compacting chracteristics of a normal Proctor test.

Note that the Proctor curve requires a minimum of 5 points.

The test method, apparatus and calculations can be found in appendix B.3.

5.3.2 Results

The results are shown on table 5.3 and figure 5.2.

Tests	$m_{wet,net}$ (g)	ω (%)	ρ_w (t/m^3)	ρ_d (t/m^3)
Test 1	3502,3	0,12	1,65	1,64
Test 2	3487,6	5,90	1,64	1,55
Test 3	3533,6	7,86	1,66	1,54
Test 4	3550,1	9,01	1,67	1,53
Test 5	3634,6	9,80	1,71	1,56
Test 6	3678,2	10,22	1,73	1,57
Test 7	3754,9	11,57	1,76	1,58
Test 8	3777,6	11,79	1,78	1,59
Test 9	3970,2	12,44	1,87	1,66
Test 10	3964,4	12,91	1,86	1,65
Test 11	3980,8	13,96	1,87	1,64
Test 12	3966,2	15,81	1,86	1,61
Test 13	3944,4	17,07	1,85	1,58

Table 5.3: Dry density of the soil during the normal Proctor test

Although the curve isn't perfect, we can clearly see on these results that the optimal moisture content of our soil is located around 12,5% of water content with a dry density of about 1,66 t/m^3. The 10% water content used to realise our test is quite far from the optimal moisture content with a dry density of about 1,56 t/m^3.

5.4 Steel interface

The interface used during the tests is made out of steel. Although the surface can look perfectly smooth, there are some irregularities that can be measured using a roughness tester. The roughness of the interface is a key parameter affecting the pipe-soil interaction, as explained in the introduction (chapter 1).

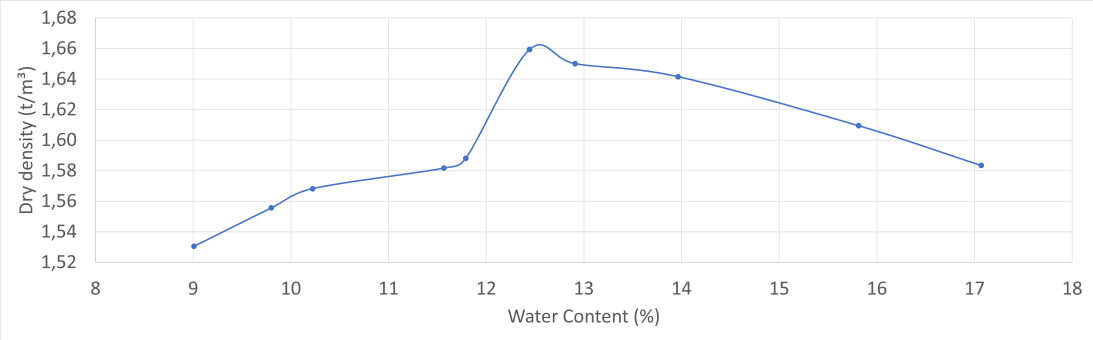


Figure 5.2: Proctor curve of the white sand

5.4.1 Roughness test

The roughness is tested by a stylus moving along the interface, measuring the variations of the heigth with a sensor. The device recreates the heigth's variation curve of the tested interface and processes the measured data to give the roughness parameters.
The roughness test was realised using a MarSurf PS10 roughness tester and was tested two times on both sides of the interface with a displacement of 4mm. The apparatus measured the average roughness R_a and the mean peak to valley heigth R_z.
R_a is the "arithmetic average of all surface heights measured over a surface." [29] Its formula is:

$$R_a = (1/L_m) \int_{x=0}^{x=L_m} |y| \, dx$$

Where L_m is the scanned length. [8]

R_z is the "average of the five biggest discrepancies between peaks and valleys across the surface." [29] Its formula is:

$$R_z = z_1 + z_2 + z_3 + z_4 + z_5$$

z_1, z_2, z_3, z_4 and z_5 are represented on figure 5.3. [8]

The tested average roughnesses are located between 1,138 and 1,525 μm. The values of R_z are located between 8,7 and 10,5 μm. The graphs of the roughness are presented in appendix C.
The values obtained show that the steel plate's roughness can be qualified of "good machine roughness/finish". [29]

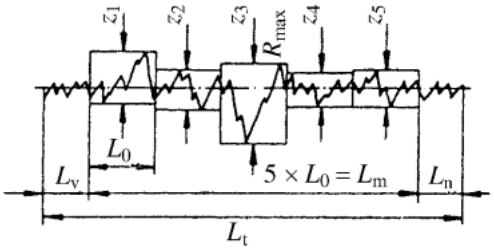


Figure 5.3: Representation of the five biggest discrepancies between peaks and valleys across a surface to find R_z [8]

Note that the steel interface isn't made out of stainless steel; it is then subjected to rust and the interface roughness might deteriorate over time. The value of the average roughness didn't change over time but we can see visibly the appearance of rust over time by comparing the pictures of the steel plate before and after all the experiments on figures 5.4 and 5.5. The photos were taken about 6 months apart.



Figure 5.4: Steel plate before the experiments



Figure 5.5: Steel plate after the experiments

5.4.2 Link with the normalised roughness

Returning to the introduction, on figure 1.3, we can see on the left of the graph that the pipe-soil resistance is affected by the normalised roughness R_n. The relative roughness is equal to the average roughness of the plate R_a divided by the mean particle size, D_{50}, of the tested soil.
Both properties were tested previously in this chapter. Taking an average relative roughness of 1,25 μm for our plate and a D_{50} of 415 μm for our sand, a relative

roughness of $3 * 10^{-3}$ is obtained. This value will be used further in the document as a point of comparison with existing datasets.

Chapter 6

Assessment of axial pipe-soil resistance

In this chapter, we are going to carry out low stress interface shear box tests on the sand and the interface described in chapter 5. Different parameters will be tested, such as the density of the sand, the axial pressure applied on the sample, the effect of long displacements,...This will be a good way to find out how the apparatus responds with the different changes and its limitations.

As explained in section 4.3.4, our results will be corrected by a stress of 0,5 kPa. This correction will have a bigger or lower impact depending on the axial pressure applied.

The shearing speed during the tests will be 0,45mm/min for each test, as it is the usual shearing speed used to realise the direct shear tests and it is lower than the hydraulic conductivity of the sand (section 5.1.3), in order to stay in drained conditions.

6.1 State of the art and existing datasets

The assessment of axial pipe-soil resistance was carried out by several studies, with a wide range of soils and interfaces of different properties. These experiments resulted in the development of several relationships governing this resistance. We are going to review each parameter that will be tested with the existing theory.

6.1.1 Low normal stress

"The axial resistance is affected by the pipe-soil interface roughness and the effective stress level". [9] As said in the DNVGL-RP-F114, the effect of the normal stress on the pipe-soil resistance is undeniable and is of the utmost importance.

This parameter is the main focus of the study. At very low stress, the axial resistance of soil on the interface increases as the normal stress decreases. This phenomenon can be seen on the right of the figure 6.1. This figure also shows that in drained conditions, for a given stress, we should expect the same friction coefficient if the same soil and interface are tested several times.

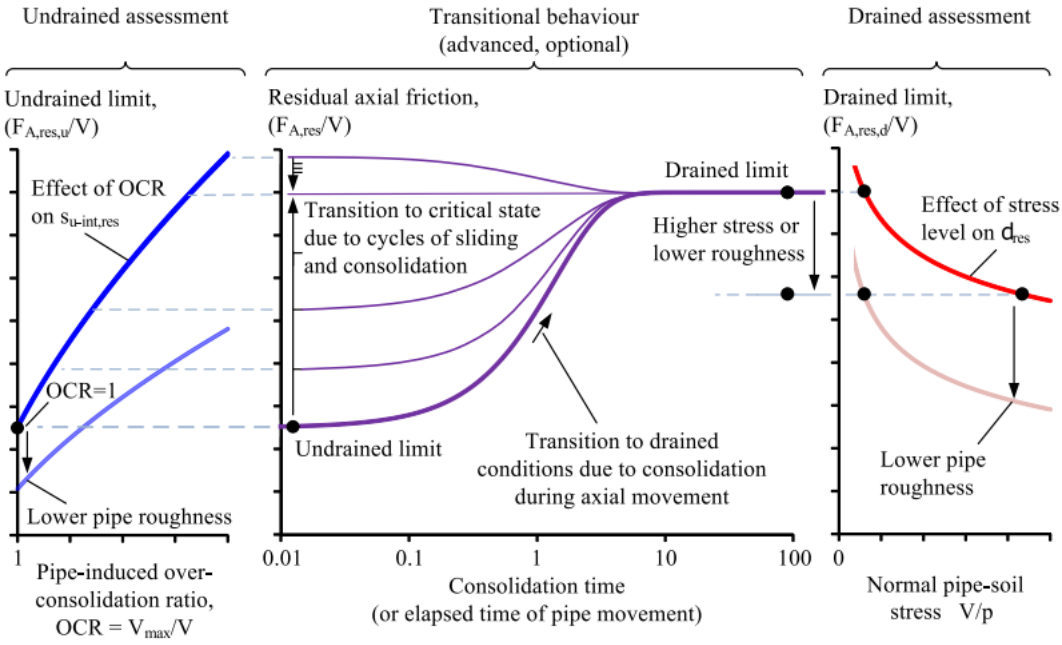


Figure 6.1: Model for axial resistance [9]

The representation of shear stress as a function of the normal stress was already presented in the chapter 1 and is shown again on figure 6.2. The relationship between the axial and normal stress can be expressed by the following formula:

$$\tau = a(\sigma'_n)^b \leq \mu_{max}\sigma'$$

Where a, b and μ_{max} are constants and specific to the studied soil.
These constants will be estimated later in the chapter. Note that the theorically soil is completely cohesionless.

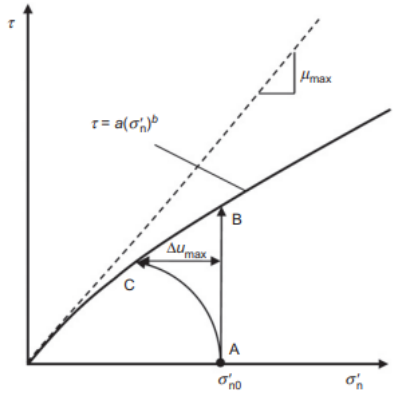


Figure 6.2: Soil-interface shear resistance as a function of the axial stress [2]

6.1.2 Sand density

One of the tested parameter is going to be the effect of the sand density while preparing the sample on the shear resistance. There is no clear study about this but as the samples are drained and submitted to the same consolidation time afterwards, we expect the same stress if we refer to the figure 6.1.

Looking at the change in sample's volume during the test, we expect a different change in volume if the sample is loose or dense. The loose sand's volume is supposed to decrease during the shearing while a denser sample is supposed to have an increase of the volume during the shearing. We also expect the denser samples to reach a maximum in shear resistance before decreasing a bit, while a loose sand reaches the maximum resistance and stays constant. [30] These phenomena are illustrated on figure 6.3.

6.1.3 Effect of long displacements

The particularity of our tests is that a push-pull loop is applied to the samples between 10mm and -10mm. This will give informations on the effect of long dispacements. The total shear length is 40 mm.

According to the DNVGL-RP-F114 [9], a recommended practice about the evaluation of the pipe-soil interaction, "the drained resistance is usually not significantly affected by large soil displacements/strains".

A similar study on long displacements was conducted by White et al, 2017 [2] on clay-interface resistance with push-pull loops but none could be found on sands.

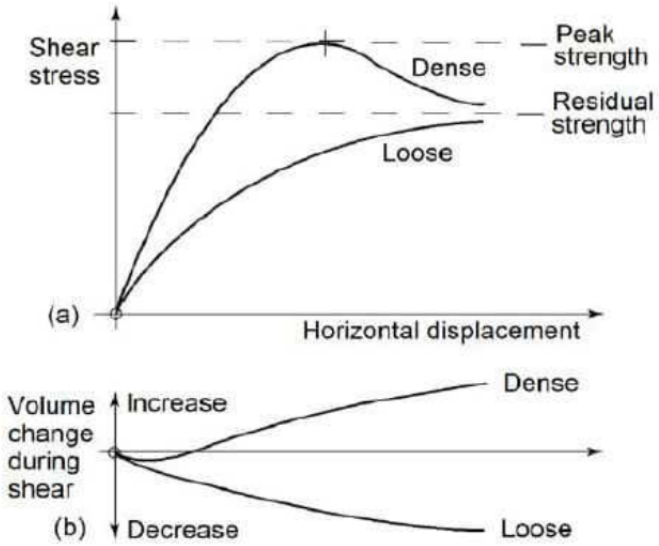


Figure 6.3: (a) Peak and residual shear strength for a sandy specimen at dense and loose state, (b) Volume change during shear for the dense and loose sand [6]

In the case of clay, the shear resistance was slightly increasing until reaching a constant value for long displacements.

6.2 Mass on sample

During the tests, a perforated plate, a porous stone and a loading cap are placed above the soil sample. The combined mass of those 3 pieces is usually located between 325 and 330g. The induced stress on the soil sample can be calculated. By taking a mass of 330 gramms, a sample surface of a 60 mm diameter circle and a gravity force of $9,81 m/s^2$ we obtain the following result:

$$\frac{0,33 * 9,81}{0,03^2 * \pi} = 1145 Pa = 1,145 kPa$$

For a mass of 325 gramms, the stress would be 1,127 kPa.

This value needs to be added to the axial pressure applied on the sample to get the real pressure applied.

6.3 Effect of soil density and normal stress

6.3.1 Tests

The first tested parameters were the effect of density and normal stress. The minimum and maximum density were measured in section 5.2. The samplewas prepared by either not applying any force or compacting it as much as possible. The same pressure was applied for both densities during the consolidation and shear stages.

The consolidation was configured to last fifteen minutes with a ten seconds ramp to reach the desired pressure. This time allows the sample to be fully drained by capillarity over its entire thickness.

As explained in subsection 4.3.4, we will substract 0,5 kPa to the obtained results due to the residual stress of the shear box.

The normal stresses tested are 5, 10 and 20 kPa. The comparison of shear stress at different density for each separate normal stress applied is shown on graphs 6.4, 6.5 and 6.6.
The separate graphs obtained for each test are presented in appendix D.1.

We can see that the shear stress graphs of both soil densities are nearly overlaid for each normal stress applied. A small difference can be seen for the graph with a normal applied stress of 5 kPa.

The mean stress of each test can be calculated to compare the tests more precisely. To do so, we will use the same technique as for the analysis of the residual stress in section 4.3.4: calculating it by taking the values from 5 to 9mm, 4 to -4mm and -7 to -3mm.
The mean stress is corrected by substracting 0,5 kPa of residual stress as explained in section 4.3.4 and the introduction of this chapter. The impact of the correction can be quantified by comparing the 0,5 kPa to the mean stress of the test. The different values are reported in tables 6.1 and 6.2.

We can clearly see on table 6.1 and figures 6.4, 6.5, 6.6 that the values obtained by preparing the sample at its maximal or minimal density are similar. The biggest difference between tests with the same axial stress and different densities is 0,68 kPa for the tests with 5kPa applied. As we can see on graph 6.4, the sand creates a lot of noise proportionally to the shearing force.

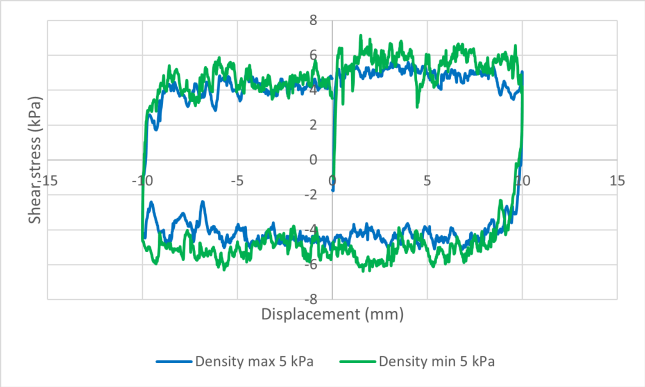


Figure 6.4: Comparison of the shear stress with 5kPa axial stress between min and max density

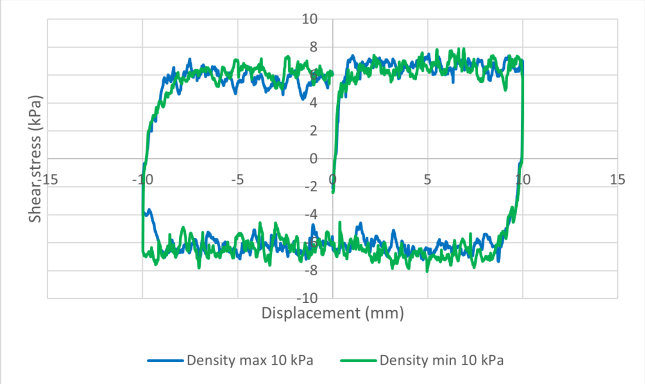


Figure 6.5: Comparison of the shear stress with 10kPa axial stress between min and max density

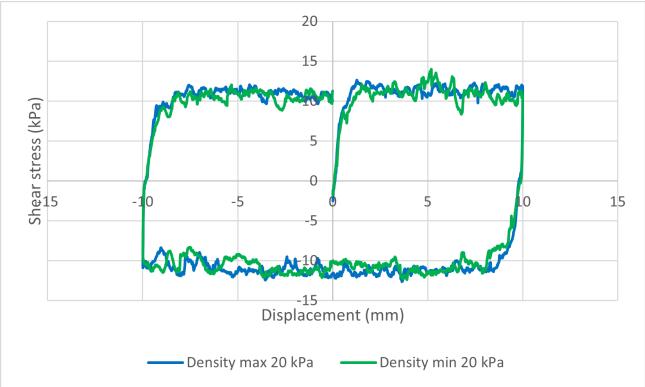


Figure 6.6: Comparison of the shear stress with 20kPa axial stress between min and max density

Test	5 to 9mm	4 to -4mm	-7 to -3mm
Density min 5 kPa	6,57 kPa	-4,16 kPa	5,63 kPa
Density max 5 kPa	6,45 kPa	-2,79 kPa	5,76 kPa
Density min 10 kPa	9,00 kPa	-4,06 kPa	8,60 kPa
Density max 10 kPa	8,15 kPa	-4,57 kPa	7,38 kPa
Density min 20 kPa	12,12 kPa	-9,99 kPa	11,87 kPa
Density max 20 kPa	13,50 kPa	-9,28 kPa	13,23 kPa

Table 6.1: Mean shear stress of sections of the sand

Test	Mean stress	Corrected Mean	Proportion corrected
Density min 5 kPa	5,13 kPa	4,63 kPa	9,75 %
Density max 5 kPa	4,45 kPa	3,95 kPa	11,24 %
Density min 10 kPa	6,43 kPa	5,93 kPa	7,78 %
Density max 10 kPa	6,17 kPa	5,67 kPa	8,10 %
Density min 20 kPa	10,99 kPa	10,49 kPa	4,55 %
Density max 20 kPa	11,32 kPa	10,82 kPa	4,42 %

Table 6.2: Mean stress, corrected mean stress and percentage of correction of the sand loop tests

The tests at max density seem to reach a peak as expected but it is very minimal.

During these tests, The change in volume for both densities during the first rise of the shear stress was compared. The results are shown on figures 6.7, 6.8 and 6.9.

We can see that the volume change is indeed lower for the denser sample but it doesn't increase for the maximum density as we expected it apart from the test at 5 kPa.

In order to visualise the effect of the normal stress on both densities, a graph of the mean shear stress as a function of the axial stress and a graph of the friction coefficient as a function of the axial stress were drawn to see if it fits the curves seen in the litterature. The graphs are shown on figures 6.10 and 6.11 .

Note that for the axial stress, a stress of 1,14 kPa was added to each axial stress to take into account the stress created by the perforated plate, porous tone and loading cap.

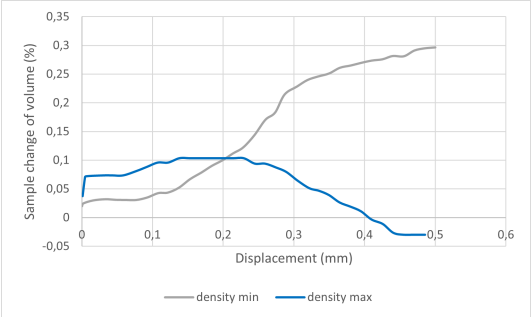


Figure 6.7: Volume change for maximum and minimum density with a normal stress of 5 kPa

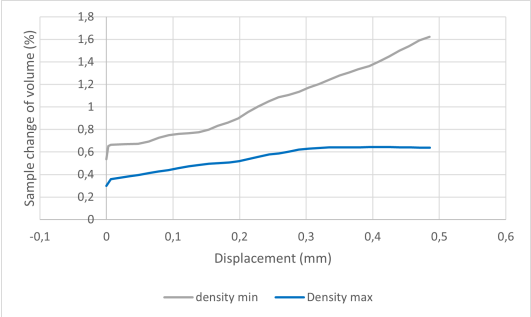


Figure 6.8: Volume change for maximum and minimum density with a normal stress of 10 kPa

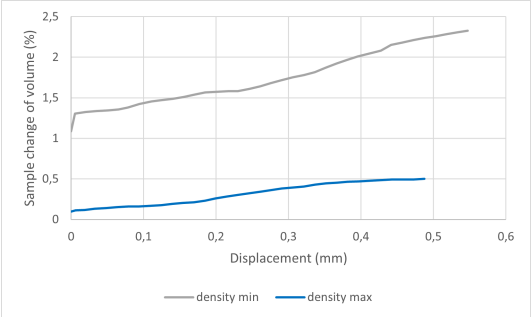


Figure 6.9: Volume change for maximum and minimum density with a normal stress of 20 kPa

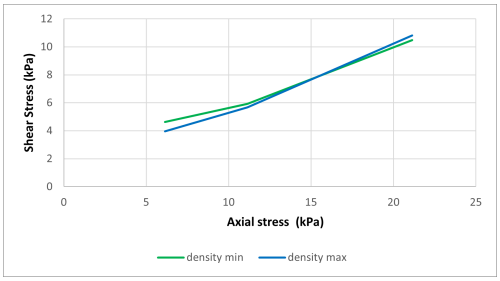


Figure 6.10: Mean shear stress as a function of the axial stress

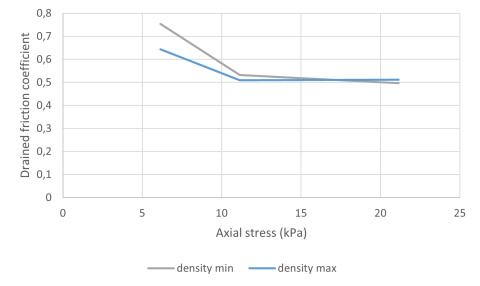


Figure 6.11: Drained friction coefficient as a function of the axial stress

The table 6.3 presents the dynamic friction coefficient of the sand for each test.

Looking at the table 6.3 and figures 6.10 and 6.11, we can see that the friction coefficient is much higher for a pressure of 5 kPa applied on the sample than

Test	Axial stress (kPa)	Shear stress (kPa)	Friction coefficient
D min 5 kPa	6,14	4,63	0,75
D max 5 kPa	6,14	3,95	0,64
D min 10 kPa	11,14	5,93	0,53
D max 10 kPa	11,14	5,67	0,51
D min 20 kPa	21,14	10,49	0,50
D max 20 kPa	21,14	10,82	0,51

Table 6.3: Dynamic friction coefficient of the sand for each pressure and density

for higher stresses applied. The friction coefficient for the 4 tests at 10 and 20 kPa applied is similar, located between 0,49 and 0,53. This proves that at low normal stress the friction coefficient is indeed higher but we can see that at 10 kPa the effect begins to wear off.

The shear stress obtained with a normal stress of 10 kPa for both densities is a bit low if we compare the shape of the theoretical graph on figure 6.2 with figure 6.10; or the values with a normal stress of 5kPa were a bit high. The same conclusion can be drawn if we compare figures 6.1 and 6.11.

Overall, the precision of the apparatus seems accurate, the difference in mean shear stress is around 0,35 kPa with a normal stress of 10 and 20 kPa. With a normal stress of 5 kPa the difference is 0,7 kPa. This difference might look small but at a such low stress, it represents a difference of about 15% and a variation of the friction coefficient of over 0,1.

6.3.2 Comparison with theory and existing dataset

In the state of the art of the chapter, the relationship between shear stress and normal stress was stated as $\tau = a(\sigma'_n)^b \leq \mu_{max}\sigma'$ with a,b and μ being constants that depend on the soil. This formula was illustrated on figure 6.2. This formula was interpolated with our results in table 6.3 and figure 6.10. This was done with the least squares method.
The comparison between the results and the corresponding interpolation are showned on figures 6.12 and 6.13.

For the minimum density, a=1, b=0,77. Note that the best interpolation would have required b$\geq$1.

For the maximum density, a=0,72 and b=0,88.

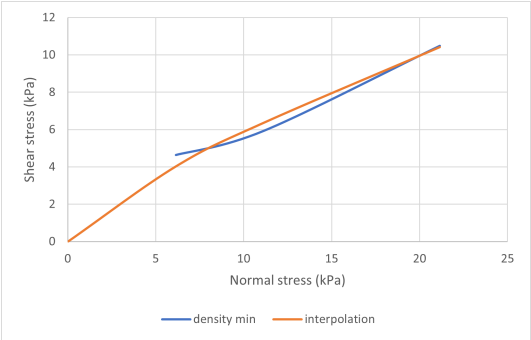


Figure 6.12: Interpolation of the shear stress at minimum density as a function of the axial stress

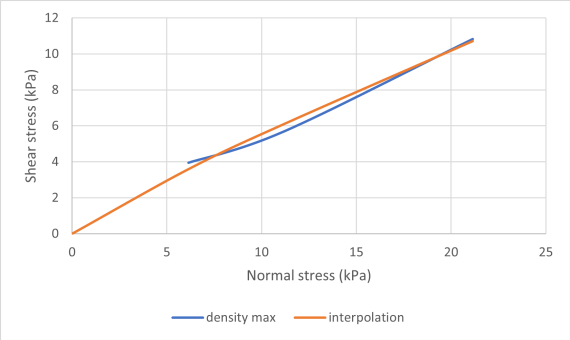


Figure 6.13: Interpolation of the shear stress at maximum density as a function of the axial stress

On both graphs, we can see that the shear stress obtained with a 5kPa normal stress is higher than the expected value and the values with a 10 kPa normal stress appear a bit lower than expected.

Westgate et al, 2021 [10] presented a dataset of results for silicate and carbonate sands with an interpolation of constants a and b. Figure 6.14 shows the mean residual stress of silicate sands at a low normal stress. The 3 lines show the relationship between normal and shear stress with the P_{10}, P_{50} and P_{90} percentiles of the constants a and b. Note that b is often taken as a constant equal to 0.9 at low stress [31]. The values of a and b are reported at the top of the described figure.

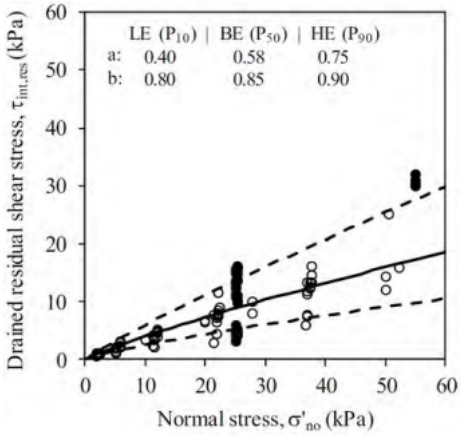


Figure 6.14: Dataset of residual stress for silicate sand at low normal stress [10]

Comparing our values of a and b to theirs, we can see that the interpolation at maximum density is in a similar range for the constant b; a is a bit high but still acceptable. At minimum density, the value of a is too high and b is a bit low. This means that the first value at 5 kPa is too high compared to the other values. The values of the shear stress obtained with a normal stress of 5kPa are below 0,5% of the load cell, which seems to be the limit to obtain a good accuracy.

6.3.3 Comparison with datasets of different average roughness

The shear stress is affected by the surface roughness of the interface. In the previous comparisons, this parameter into account wasn't taken into account while comparing the results. We are now going to see where it stands if we compare the shear stress as a function of the normalised roughness.
In section 5.4.1, we calculated the normalised roughness of our interface with our sand. We obtained a normalised roughness $R_n = 3 * 10^{-3}$.

Westgate et al, 2021 also provided datasets of silicate sands tested on different interfaces, comparing their friction coefficient as a function of the normalised roughness. These datasets are provided on figures 6.15 and 6.16. The normal stress applied during the tests shown on figure 6.15 is located between 2 and 70 kPa.

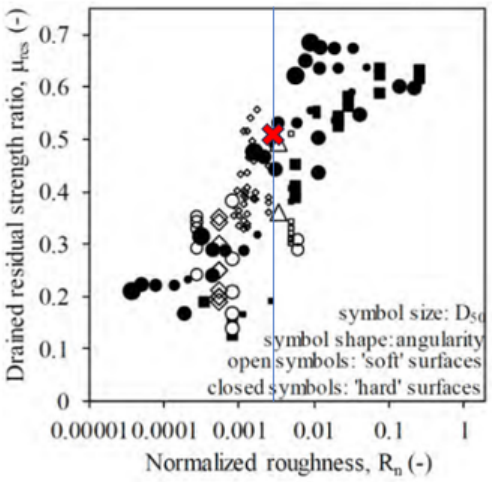


Figure 6.15: Dataset of silicate sands comparing friction coefficient as function of the normalised roughness [10]

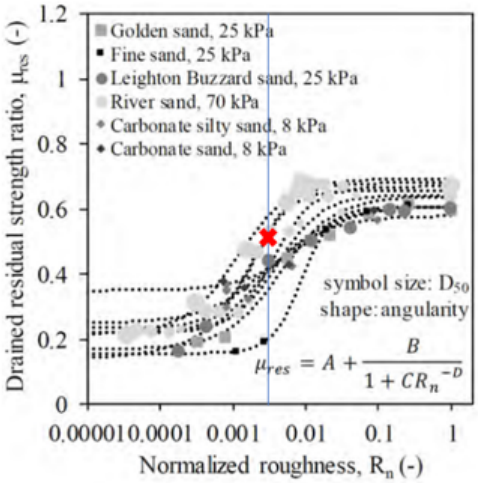


Figure 6.16: Dataset of silicate sands comparing friction coefficient as function of the normalised roughness [10]

The normalised roughness of our tests is represented by the blue vertical line on both figures. The red cross represents our result with a normal stress of 10 kPa. This value was chosen because it's similar for both densities and not far from the values with a normal stress of 20 kPa. In addition, the accuracy of the tests with a 5kPa normal stress can't be trusted enough, as explained in the previous subsection.

We can see that our results are in the range of the dataset, in the highest part for this given normalised roughness. The figure 6.16 shows that our value for the normalised roughness is in the transition part between smooth and rough.

6.4 50 kPa normal stress test

To confirm the results in subsection 6.3.2, a test with an axial stress of 50 kPa (at max density) was run. The graph obtained is shown on figure 6.17. The calculation of the shear stress is reported in table 6.4.

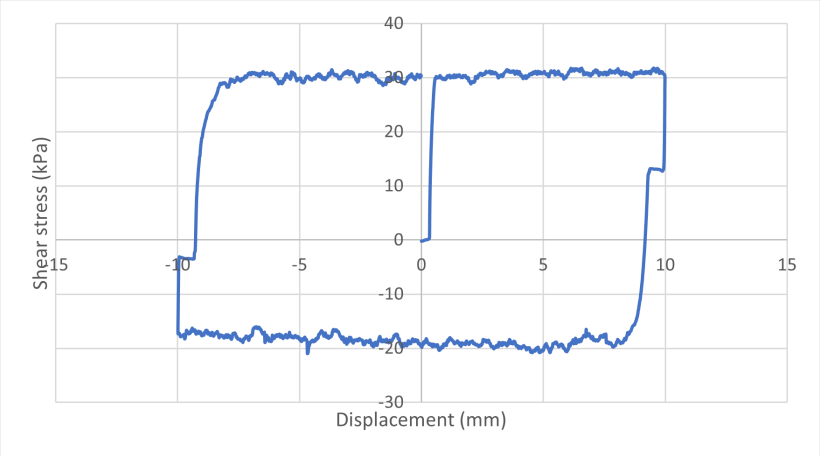


Figure 6.17: Shear stress 50 kPa max density

Test	5 to 9mm	4 to -4mm	-7 to -3mm	Mean	Corrected mean
D max 50 kPa	30,88 kPa	-18,86 kPa	30,24 kPa	24,71 kPa	24,21 kPa

Table 6.4: Mean shear stress of the sand at max density with 50 kPa of axial stress

This gives us a dynamic friction coefficient of 0,47. Compared to the values obtained in table 6.3, it is slightly lower than the friction coefficient obtained with an axial stress of 10 and 20 kPa, confirming the theory that the friction coefficient

is higher at very low stress. The overall results can be illustrated by the shear stress as a function of the axial stress for the samples prepared at the maximum density of the sand and friction coefficient as a function of the axial stress. The graphs are shown on figures 6.18 and 6.19.

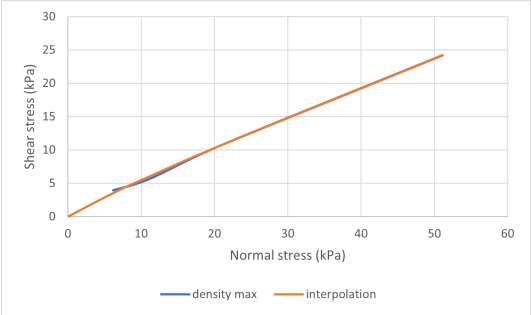


Figure 6.18: Mean shear stress as a function of the axial stress at maximum density

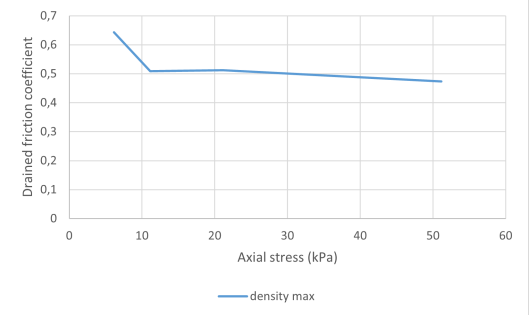


Figure 6.19: Evolution of drained friction coefficient as a function of the axial stress

Compared to the theoretical figure 6.1 and the previous graphs in subsection 6.3, this test confirms that we do have a decrease of the friction coefficient when the normal stress increases.

The interpolation of the results with the formula $\tau = a(\sigma'_n)^b \leq \mu_{max}\sigma'$ shown on figure 6.18 give us a=0,67 and b=0,91. These values are close to the ones obtained with the interpolation of only 3 points on figure 6.13 (a=0,72 and b=0,88), proving again that the results and the theory are in accordance.

6.5 Effect of large displacements

Another point of study of this document was the effect of long displacements on the shear stress between the soil and the interface. To do so, some tests doing two push-pull loops were run to see the changes between both loops. Two different tests were run, one with a normal stress of 5 kPa and another one with a normal stress of 14,1 kPa. These tests are represented on figures 6.20 and 6.21.

The table 6.5 presents the detailed results of each loop.

We can see on the graphs that the first shearing between 0 and 10mm is higher than the second one. Looking at the results in the table, we can see that usually

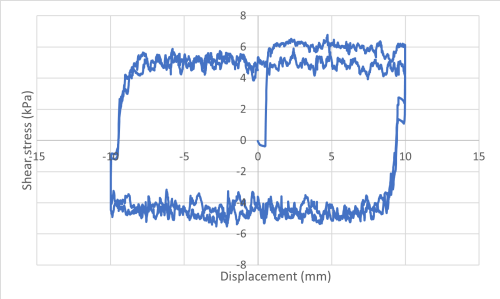


Figure 6.20: 2 loops 5 kPa normal stress

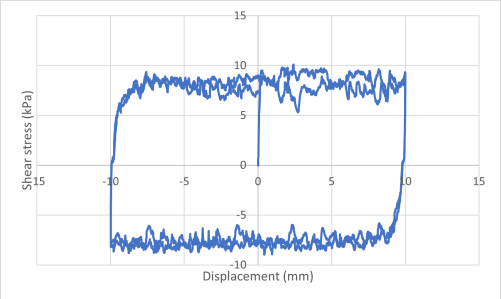


Figure 6.21: 2 loops 14,1 kPa normal stress

Test	5 to 9mm	4 to -4mm	-7 to -3mm	Corrected mean stress
5kPa loop 1	5,89 kPa	-4,36 kPa	5,03 kPa	4,41 kPa
5kPa loop 2	4,75 kPa	-4,69 kPa	5,08 kPa	4,3 kPa
14kPa loop 1	8,53 kPa	-7,76 kPa	8,22 kPa	7,57 kPa
14 kPa loop 2	7,63 kPa	-7,59 kPa	8,11 kPa	7,28 kPa

Table 6.5: Mean shear stress of each loop during 2 loops tests

the first loop has a higher shear resistance in severy sector, but overall there is just a small difference looking at the mean stress of the whole loop.

We can conclude that the long displacements don't impact much the results, as it was planned by the theory in section 6.1.

6.6 Confirmation of drained conditions

As explained at the beginning of the chapter, a shearing speed of 0,45mm/min was chosen and the assessment that the test would be perfectly drained at this speed was made because it was a lower speed than the hydraulic conductivity, calculated using Hazen's formula in section 5.1.3.
In order to confirm this assessment, a test was realised at a speed of 0,1mm/min. The axial stress applied was 20 kPa.

The figure 6.22 shows the comparison between both shearing speeds.

The mean corrected shear stress at 0,45mm/min is equal to 10,82 kPa and 11,01 kPa at 0,1 mm/min. As we have a similar result, this proves that all the tests carried out at 0,45mm/min were fully drained and that the shearing speed doesn't affect the results in fully drained conditions.

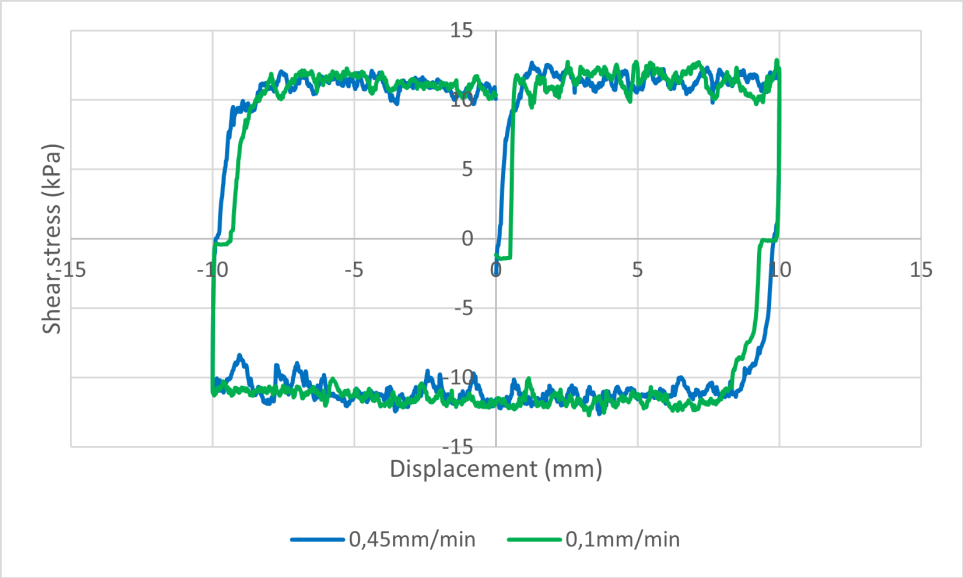


Figure 6.22: Comparison of the shearing speed at 20 kPa

6.7 Imperfections during the tests

If we look at the graphs of the push-pull loops, for example the test with a normal stress of 50 kPa on figure 6.23, we can see three different kind of imperfections on the graph.

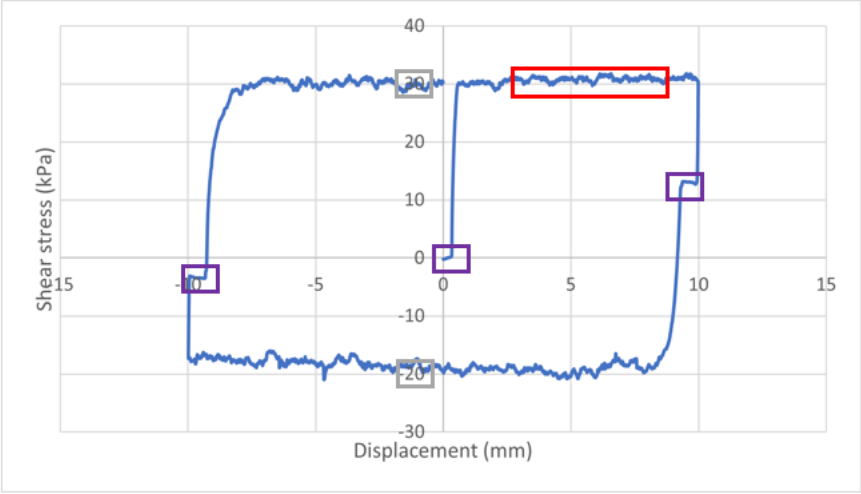


Figure 6.23: Visible imperfections on shear stress vs displacement graphs

The first one is the vibrations during the tests (in red on the graph). This imperfection is caused by the sand and was already visible in chapter 4.

Another imperfection is the plateau that we sometimes notice at the beginning of the shearing and during the changes of direction. It's represented in purple on figure 6.23. This is due to the way the nut of the apparatus is tightened (cfr figure 8 in appendix A). To give the horizontal bar connected to the load cell the ability to move freely, the nut isn't screwed to the maximum, as explained in subsection 3.1.3.

Finally, the last visible imperfection is the decentering of the graph. As we can see with the shear stress values circled in grey on the graph 6.23, the shear stress in the forward direction is higher than in the backwards direction This problem led to further investigations. No documentation was found on the subject.

6.7.1 Decentering during the tests

We can see on every graph presented that each loop is never perfectly centered and that there is a shift between the results of the forward shearing and backwards shearing. To make sure the shear direction isn't the cause of this problem, some tests were run by going backwards first, but the tests were still decentered with a bigger shear stress on the way forward. The resulting graphs can be seen in appendix E.

Based on the values of the shearing between 4 and -4mm and the mean of the total loop presented in table 6.2, the value of the shift for each loop of our tests can be calculated. The table 6.6 presents these values for the 6 tests between 5 and 20 kPa at both densities obtained earlier in the chapter .

Test	Shift (kPa)
D min 5 kPa	0,97
D max 5 kPa	1,66
D min 10 kPa	2,37
D max 10 kPa	1,60
D min 20 kPa	1,00
D max 20 kPa	2,04

Table 6.6: Shift of each loop

An hypothesis was that this decentering could be linked with the fact that before

applying any stress, the initial stress displayed on the screen of the apparatus wasn't set to 0 even though no load was applied.
Two graphs linking the initial load displayed and the final value of the decentering were realised. They are shown on figures 6.24 and 6.25.

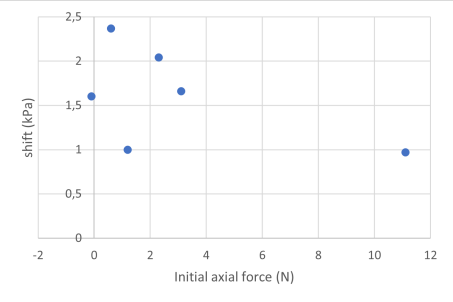


Figure 6.24: Decentering as a function of the initial axial force displayed

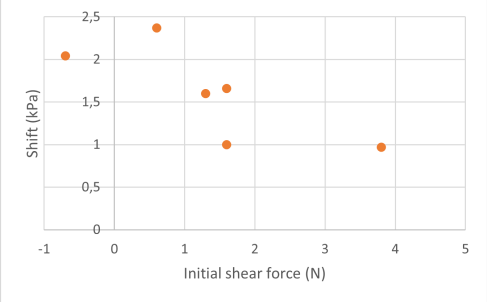


Figure 6.25: Decentering as a function of the initial shear force displayed

We can see that there is no link between these parameters.

The last hypothesis tested was that the decentering is linked with the axial stress applied. To test it, we gathered the decentering data of every tests and compared it with the axial stress applied on a graph. It is shown on figure 6.26. The tests at 0 kPa were run without a soil sample.

We can see that the decentering has the tendency to increase as the axial stress applied increases. The linear trendline is shown on the graph but the decentering can vary a lot with the same normal stress applied.

No other tests were carried out and the origin of the decentering remains unknown.

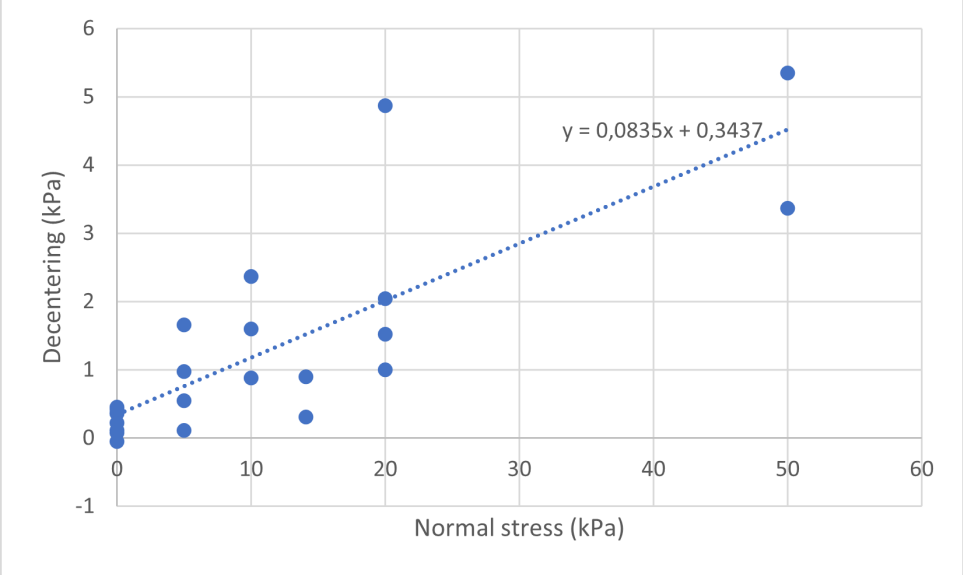


Figure 6.26: Decentering as a function of the applied axial stress

Chapter 7

Conclusion

Present work

The interface shear box tests offer a straightforward and efficient approach for evaluating axial pipe-soil interactions at very low stress. The final apparatus developped in Fugro's laboratory is able to carry out interface-soil tests and obtain accurate results at a defined range of normal stress.

In this thesis, we saw the different modifications needed to transform a usual soil-soil direct shear apparatus to a soil-interface apparatus and the difference in software setup and sample preparation to perform these tests.

The residual stress created by the friction between the upper and lower parts of the shear box, initially over 1kPa on average, was reduced to 0,5kPa with the application of Teflon sheets on both parts of the shear box. This final residual stress closely aligns with values from existing equipment. The manufacturing of a lighter upper part of the shear box could reduce this value a bit more, even though it was proven in this document that this modification should only have a minor impact.

Experimental evaluations utilizing a steel interface and white sand, all conducted under drained conditions, have showcased the apparatus's performance at low stress levels. The accuracy of the load cell around 1% of its capacity proved to be higher than expected even though the setup showed some limitations in its accuracy around 5 kPa. The results obtained at stresses between 5 and 20 kPa were in accordance with the theory and existing datasets: the friction coefficient was indeed becoming bigger as we reduced the normal stress applied on the sample. We were able to give an estimation of the formula linking the axial and shear stress of our soil and interface. For dense samples we obtained $\tau = 0,72(\sigma'_n)^{0,88}$, which is in the expected range.

The effect of other parameters was also studied. The sample's density was proven to have no impact on the shear resistance and the large displacements didn't affect much the results either, in accordance with the theory.

Some imperfections appeared in our tests results and an analysis was realised for all of them to explain their cause. They don't affect the mean shear stress obtained. The vibrations in the results are explained by the sand particles moving during the shearing process and can't be avoided. The plateaus appearing at the beginning of the shearing and changes of direction come from the screwing of the connection between the horizontal bar and the load cell. These can be avoided by completely screwing both parts, but it is not recommmended in the procedure as it doesn't allow the bar to move freely. Finally, the decentering of the results was proven to be linked with the normal stress applied but no solution to avoid it was found.

Future perspectives

The present work and its conclusions can lead us to some perspectives and recommendations in order to get an even better accuracy and efficiency of the tests.

Although the residual stress was reduced to 0,5 kPa (similar to other existing apparatus); this value could be considered high if we work at extremely low stress. If this residual stress is ever found problematic for the application of future tests, the shear box could be manufactured with a lighter component to reduce the residual stress and the total weight of the shear box. This hypothesis is based on the fact that the residual stress should come from the friction coefficient beetween both parts of the shear box and the weight of the upper part. It was shown in this document that applying more weight didn't impact much the residual stress, but it is worth giving it a try if this problem ever comes up.

In the actual setup, the shear box weighs around 4,5 kg and no scale in Fugro's laboratory has the capacity to weigh it. Furthermore, as explained in the document, the interface plate doesn't fit perfectly into the lower part of the shear box and had to be fixed with 2 plastic pieces.
The manufacturing of a new lower part of the shear box could allow a better fit for the interface plate as it would no longer need to be fixed with plastic pieces.
A lighter material should make it easier to manipulate and enable to weigh the whole shear box on the actual scales. The same conclusion can be drawn if the material of the upper part of the shear box is lighter too.

We saw in this thesis that at 5 kPa, the accuracy of the apparatus wasn't very precise as our results presented more variability, but we didn't run enough test to quantifiy precisely the accuracy at such stress. Running a serie of tests for each normal stress applied would be a good way to assess the accuracy of the setup for these different levels of stress.
If the obtained values are not accurate enough for further use, the installation of lower capacity load cells could improve the accuracy at low stresses. Indeed, the actual horizontal load cell is working under 1% of its capacity at very low stress and the lower the stress applied on the load cell compared to its capacity, the less accurate it becomes in theory.

Appendix A

Direct shear procedure Fugro

1. Objectives

The present document aims to be the reference for the technicians who are performing shear box tests. To serve as the guide to be looked at and consulted when Shear box are performed.

2. Scope

The test aims to determine the shear angle (angle of friction) using the small (60x60mm square or 60mm ø) direct shear box apparatus. This is achieved by one half of the box sliding along another with a normal load and horizontal shearing force applied.

3. Related Documents

- ISO 17892-10
- Head, K. and Epps, R. (1992). Manual of soil laboratory testing. London: Plymouth: Pentech Press, pp.509-5010.
- EUAF-FGBM-SOIL-FO-408a - ShearBoxes_Square
- EUAF-FGBM-SOIL-FO-408b - ShearBoxes_Round
- Clisp Studio software and VJ Tech ring shear user instructions.

4. Responsibilities

People trained and authorised to perform this type of test can undertake the task.

5. Health and Safety

Always wear steel toe cap boots when compacting the samples.

Wearing plastic gloves when handling samples can prevent contamination and protect hands. A lab coat is always suggested.

Especially for when samples are being compacted ear plugs and safety glasses should be worn.

6. Apparatus and Reagents

6.1 Apparatus

- SSP: Shear Scan Pro – shear box apparatus
- Digital Calliper
- Shear box moulds with different interfaces and plates (soil : soil / soil : steel)
- A steel cube, wooden dollies, and dead blow hammers for the compaction
- Pallet knife
- Plastic water disposer
- Water jug
- Little tray

- Water content tins
- Calculator
- Trolley

6.2 Reagents

N/A

7. Test method

7.1 Equipment checks

- Ensure that all equipment used are within calibration.
- Verify that the balances used have been checked and results are recorded on EUAF-FGBM-SOIL-TM-115a-Daily check of Balances.
- All equipment should be clean prior to use. A visual check for obvious damages of malfunctions is made before every test on all used equipment.
- Generally, ovens operating between 105°C and 110°C should be used. If organic matter is present in high quantities, then sample should be dried at 50°C.

7.2 Sample and equipment preparation

The test is carried out on soil previously dried in the oven for 24 hours at 110 ° and sieved on 2.0 mm sieve. If any particles are larger than 2mm you will have to pass it through the 4mm sieve and make sure that the 2-4mm particles are also tested. Particles larger then 4mm can be crushed so they do pass the 4mm sieve. If any material is retained on the 2mm sieve, this should be recorded. The largest grains size should not be bigger then 1/6 of the sample height. Each test comprises of 3, sometimes 4 stages which will be tested on the same SSP machine. The test consists of different steps: compaction, consolidation and shearing.

First, adjust the moisture content by weighing the sample and adding the required water mass to meet the wet density mass (i.e. if it is 10% the final mass of water and dry sample should be 1.1 of the dry sample mass). We need to calculate the bulk density which is dry density x water content. Work out the volume of the mould you are going to use then times the bulk density by the volume to work out the mass needed for the test. When working out the volume, the sample hight should be about 24mm. Record the length, breadth or diameter on the sheet using the digital calliper. Weigh the top cap, porous stone and metal plate and record on the sheet. Put the bottom disc in, then the porous disc and finally the porous stone then weigh the assembled shear box on a balance.

7.3 Compaction

The compaction is the same for both round and square shear boxes. The required sample mass needs to be divided into equal sub samples either in three trays or three separate bags. Add the first portion into the shear box and measure the height using a digital calliper. Repeat this with the next two portions scarify the surface in between layers measuring each layer until the

final layer is about 24mm, each layer should be equal to each other. Weigh the sample and check the bulk density, this should be with in 0.02 of the calculated dry density.



Fig. 2. Measuring the 25 mm height

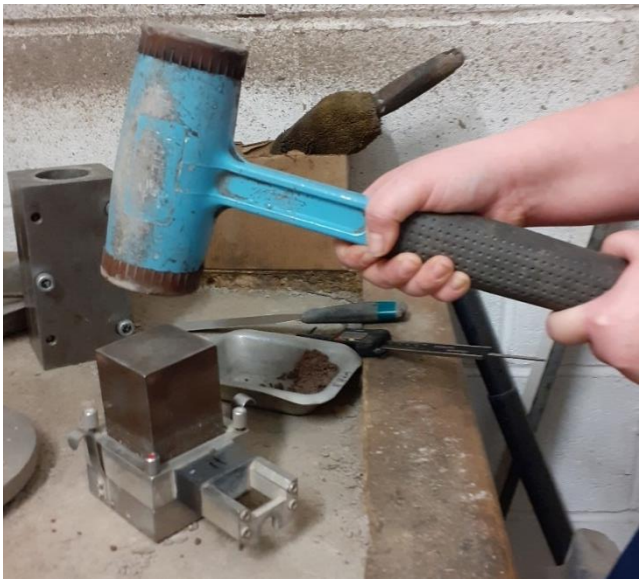


Fig. 3: Compacting the sample with a hammer and steel cube.

The required density will impact on the way the compaction should be performed. For low densities, the wooden dolly should be used with light strikes of a hammer, whereas high density sample will require the use of a steel block. (Fig 3). The latter should be done on a hard surface like the concrete plinth. Each subsequent portion of the material will typically require more strikes. (i.e. 5-7-10).

7.4 Software setup

Set up a record for your sample in the data base using Clisp software. Create the Client, Job file number, Borehole number, Sample number and the test name (i.e. SB01) based on the Test Pressure sheet data. (Fig. 4) Remember to check whether your client exists in the data base already.

Subsequently, open the Assistant wizard, choose the number of stages you are going to run and open the hardware setup to select which machine you will be running. Copy them across all the specimens (Fig. 5). **When setting up a new test make sure ISO is picked from the standards drop-down menu.**

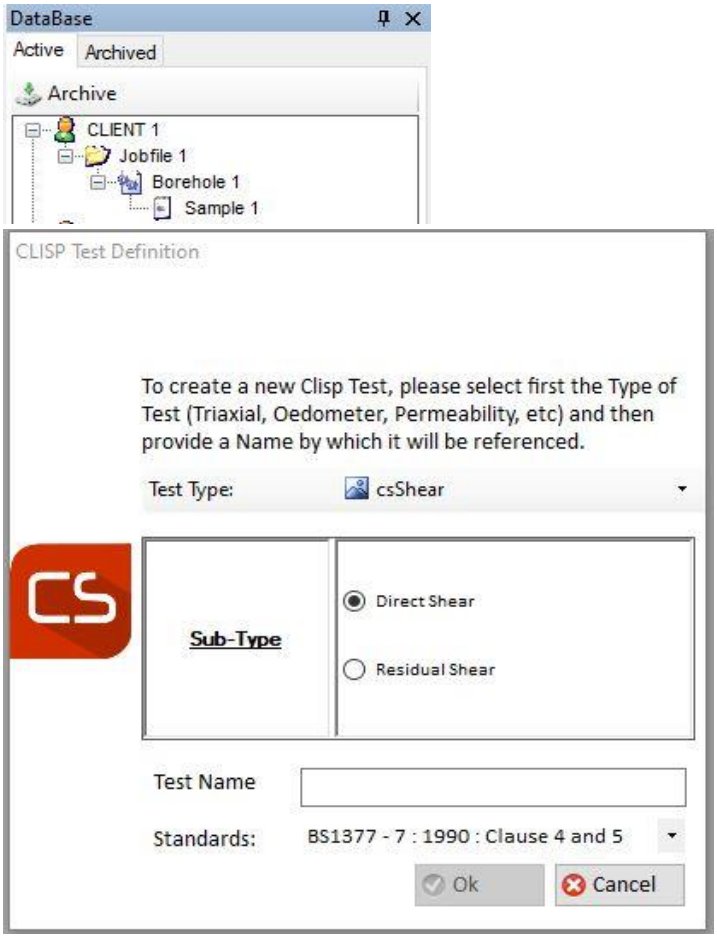


Fig. 4. Creating a sample record in the data base.

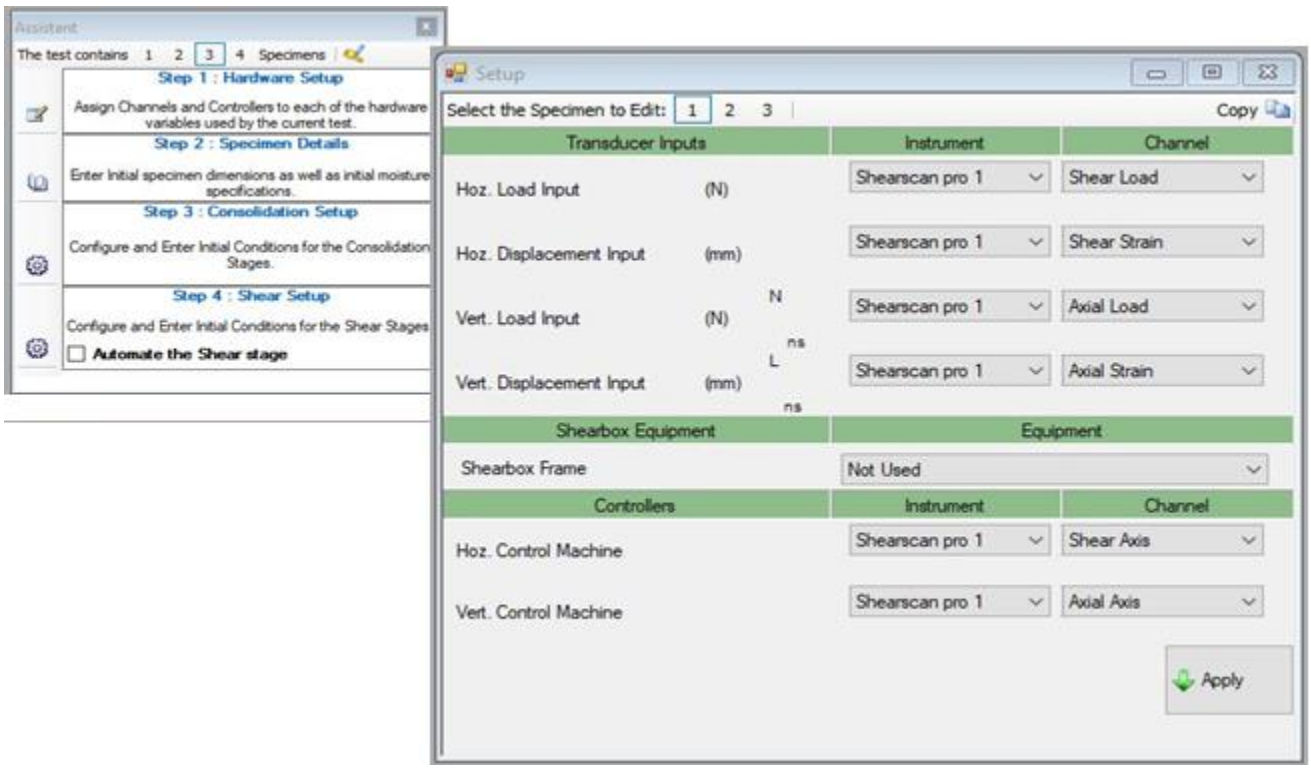


Fig. 5. Setup for the stages and hardware.

Populate the sample's initial measurements, consolidation and shear stages' parameters (Fig 6a, 6b. 6c). Make sure the dry density you aimed for is within 0.02 of the required. Usually the shearing parameters applied are:

- 0.450 mm/min is used for most of the time for the rate of displacement
- 0.01 N change for the shear load to trigger
- 10 mm/min for the reverse speed
- 5 sec for the data storage
- stop shear when the shear strain extends 18% (about 10mm)

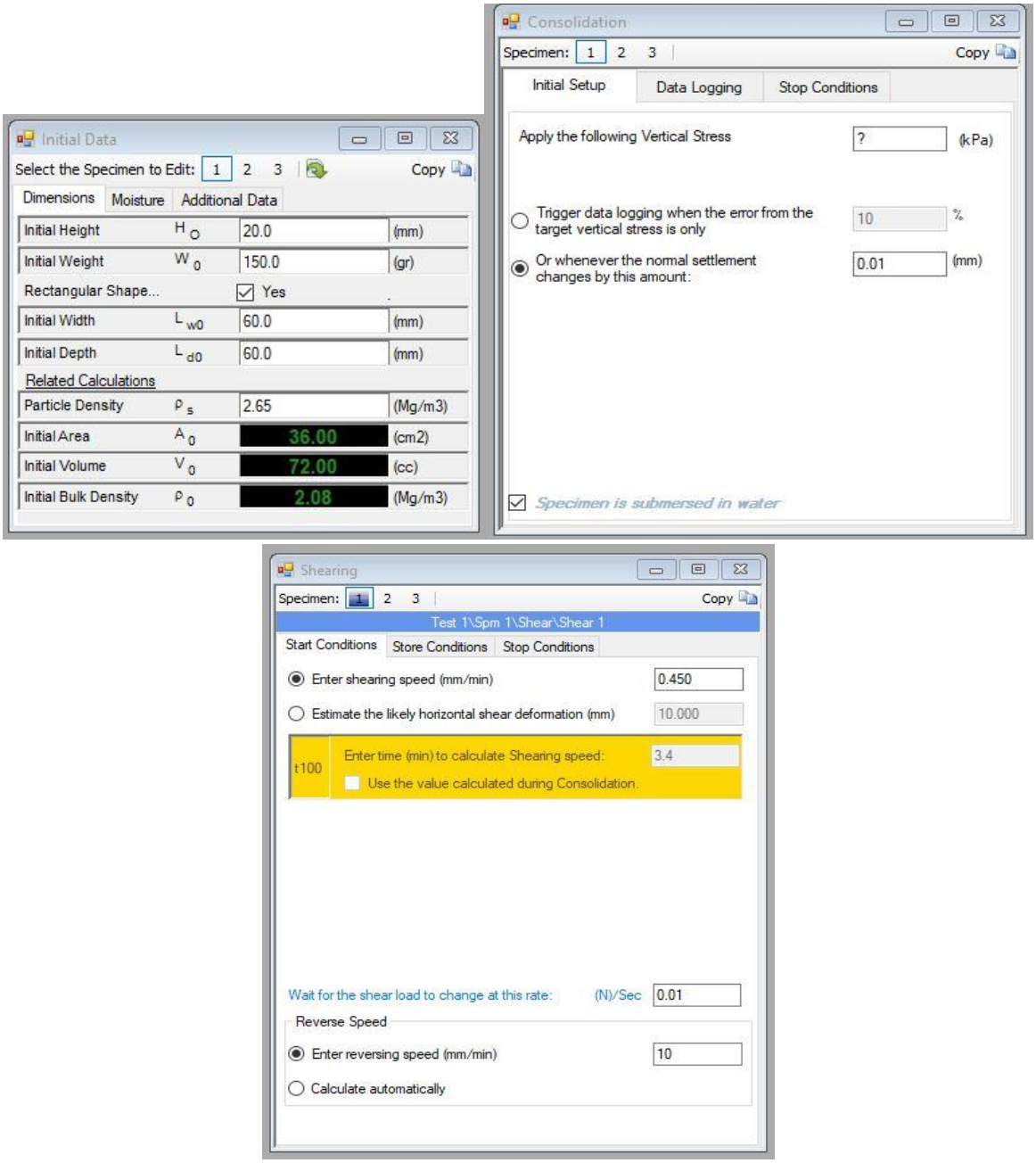
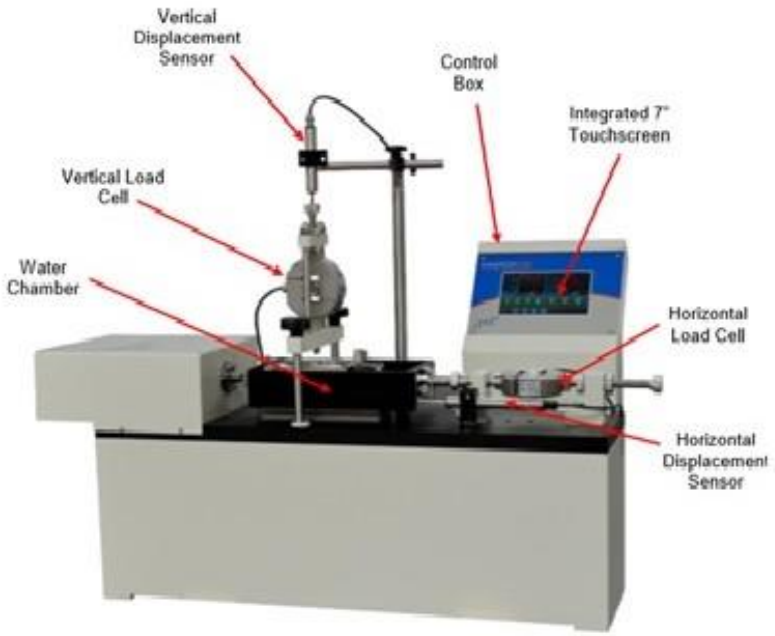


Fig. 6a. 6b. 6c. The initial setup examples.



7.5 Consolidation stage

Zero the loadcells using the Clips, this might need doing for each test.

Place the sample into the machine, with the porous stone, porous disc and top cap in place, setup the loadcell and LDT then press 'engage' button, this will apply a seating load. The consolidation data should be stored using square root times table and stop conditions are set for 18 min. **This will need changing if doing clay samples as the consolidation and shearing times will be longer.** Once the parameters are set up for the consolidation, record the start time, initial vertical load, and displacement before releasing the 'run' button.

The stress will be applied immediately, and this is when you need to add water from the jug to submerge the sample. Tap water is used.

Record the end time, vertical load and vertical displacement of the consolidation, work out and record the t100 value.

7.6 Shear stage

While holding the normal pressure, connect the box with the horizontal load cell – the first red arrow needs to be tightened so that it's connected to the loadcell (Fig. 8). The initial horizontal stress should be positive, not more than 10N especially when applying low vertical stress. Make sure the nut with the yellow arrow (third arrow) is tightened by hand then turned back less then quarter of a turn, this will allow the horizontal bar to always move freely. Unscrew the red pins from the shear box, unlocking the too halves of the box, (Clips will give you a warning as

a check before shearing starts) drive the other screws down until a you see a small gap between the boxes (this should not exceed 1mm) then back them off so they are not touching the lower box. Record the vertical and horizontal loads and the displacements on the test form.

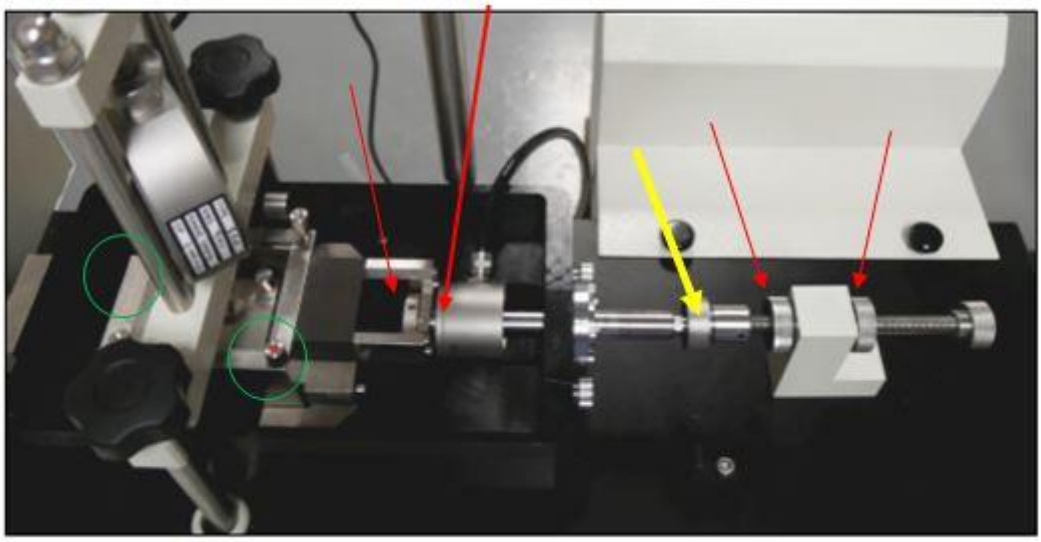


Fig. 8. Connecting the horizontal load for the shear stage.

7.7 Unloading the sample

Once the shearing stage is finished and the sample has reversed, drain the water from the carriage either by the tap on the carriage or the use of a bottle to suck the water up and allow the water to drain from the porous plates. Unload the loadcell and disconnect it. Remove the sample and take a final water content.

8. Cleaning and maintaining machines

At the end of each working day the machines should be wiped down, at the end of each week the carriage should be dismantled and toughly cleaned of any sand, software turned off and compaction area cleaned too.

9. Differences from BS 1377

If needed the present method can also be applied if BS1377 standard is required for shear box tests.

Appendix B

Characterisation of the sand

B.1 Particle size distribution (PSD) of the sand

B.1.1 Apparatus

- Sieves
- Mechanical shaker
- Brush, paintbrush
- Scale
- 105°C Oven
- Washing dispositive

B.1.2 Test method

Determination of the dry mass of the sample

The sample is weighted on a scale to determine the wet mass of the sample, then dried into the 105°C oven. Once the sample is completely dry, the sample is weighted a second time and it gives us the dry mass of the sample (M_s).

Washing

The washing of the sample aims to remove the fines of the sample that could attach to bigger grains and block the sieves.

The sample is first soaked into water. The humid sample is then poured on

one or multiple sieves to clean the sample. The sieve size is equal to the smallest sieve during the sieving part ($63\mu m$ in our case). The sample is then washed in the sieve until the water passing through the sieve is completely clear. The washed sample is then dried a second time in the oven.

Sieving

The dried and washed sample is poured into the sieve column. This column is made of the different sieves nested with decreasing sieve size from top to bottom. Place the column on the mechanical shaker during 10 minutes.

Weighing

Weigh the grains on the biggest sieve. Reiterate this operation for all the other sieves and report their mass and cumulated mass. Then record the mass at the bottom of the column.

B.1.3 Result table

The different reported masses can be analysed to obtain the PSD curve.

The different cumulated masses R_i can be devided by the dry mass of the sample (M_s).
The percentage of grains passing through the sieve can then be calculated using the following formula:

$$100 - (\frac{R_i}{M_s} * 100)$$

Our test gave us the following dry mass:
M_s = 212,76 g

The results of the sieving are presented in table B.1.
The mass passing through the $63\mu m$ sieve wasequal to 0,01 g.

B.2 Maximal and minimal density test

B.2.1 Apparatus

- Scale
- Cylindrical mould

Sieve size (mm)	Mass retained (g)	Percentage passing (%)
3,35	0,00	100,00
2,00	0,00	100,00
1,18	0,00	100,00
0,63	2,31	98,91
0,3	184,62	12,14
0,212	17,74	3,8
0,15	5,15	1,38
0,063	1,42	0,71

Table B.1: Percentage of grains passing through the sieves after the sieving

- Extension of the mould
- Leveling ruler
- Funnel
- Overload
- Brush
- Container

B.2.2 Test requirements

The test aims to determine the maximum and minimum densities of non-cohesive soils.
This test applies to natural soils with a maximum diameter of 50%. The percentage passing through a 31,5 mm squared sieve should be superior or equal to 70% and the percentage passing through a 80μm quared sieve should be inferior or equal to 12%.
In our case, the sand fullfills the requirement as you can see on the granulometry curve.

B.2.3 Test Method

Soil preparation

Dry the soil into a 105°C drying oven. Determine the quantity of soil needed depending on the choice of the mould. In our case, we used a Proctor mould with the following dimensions, measured with a digital caliper:

Dimension	Value
Heigth (mm)	116
Diameter (mm)	100,75
Volume (cm^3)	934,78
Mass (g)	3512,5

Table B.2: Dimensions of the mould.

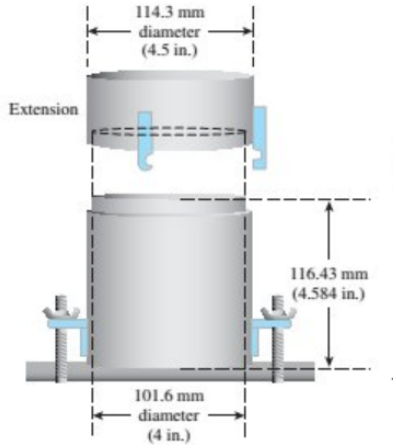


Figure B.1: Proctor mould.[11]

Determination of minimal density

The test has to be realised at least 5 times with the following procedure.
As we are working with a sand we have to fill the mould by spread method.

1. Weight the empty mould.
2. Place the extension of the mould
3. Start pouring the soul in the funnel with the funnel in contact with the bottom of the mould and make sure that there is almays enough sand in the funnel so that the soil grains don't have any drop heigth. Raise slowly the funnel to fill the whole mould.
4. Once the mould is full, remove the extension mould and use the leveling ruler to remove the soil above the heigth of the mould. Use the brush to remove the grains outside of the mould.
5. Weigh the mould with the soil in it.

Determination of maximal density

1. Weight the empty mould.
2. Place the extension of the mould
3. Pour the sand in layers and use an overload of the same diameter of the mould to compact each layer. Once the mould is full, remove the extension mould and use the leveling ruler to remove the soil above the heigth of the mould. Use the brush to remove the grains outside of the mould.
4. Weigh the mould with the soil in it.

B.2.4 Calculations

For each test, the dry density is calculated as follow:

$$\rho_d = \frac{m_d}{V_d}$$

With:
m_d the dry mass of the soil sample ($m_d = m - m_m$),
V_m the volume of the mould,
m the mass of the mould filled with sand,
m_m the mass of the mould.

The results of the different tests can be found in table B.3.

Datas	Test 1	Test 2	Test 3	Test 4	Test 5
Total mass min density (g)	4890,8	4897,5	4897,2	4906,1	4904,7
Soil mass min density (g)	1378,3	1385	1384,7	1393,6	1392,2
Total mass max density (g)	5043,2	5049,3	5064,2	5042	5064,7
Soil mass min density (g)	1520,7	1536,8	1551,7	1529,5	1552,2

Table B.3: Mass of the minimum and maximum density tests.

By convention, the density is the arithmetic mean of the different tests.

For the maximum density, if the difference between the tests and the mean value is superior to 2%, a new test should be made. It is not the case for the previous tests.

B.3 Normal Proctor test

B.3.1 Apparatus

- Compacting base
- Mould (fig B.2)
- Extension of the mould (fig B.2)
- Compaction tamper (fig B.3)
- Leveling ruler
- Scale
- Brush
- Measuring beaker

In our case, the mould chosen is a CBR mould with the following dimensions, measured with a digital caliper:

Dimension	Value
Heigth (mm)	116,5
Diameter (mm)	152,25
Volume (cm^3)	2112,4
Mass (g)	5042,1

Table B.4: Dimensions of the CBR mould.

B.3.2 Test method

This test appllies to grains of maximum 20 mm.

1. Prepare a large quantity of the tested soil.
2. Dry the soil to obtain a water content of 0%.
3. Add the quantity of water required to obtain the desired water content. Mix the sample and let it rest in a waterproof bag for at least 24 hours to make sure the water is well distributed in the sample.
4. Weight the mould before puting soil in it.

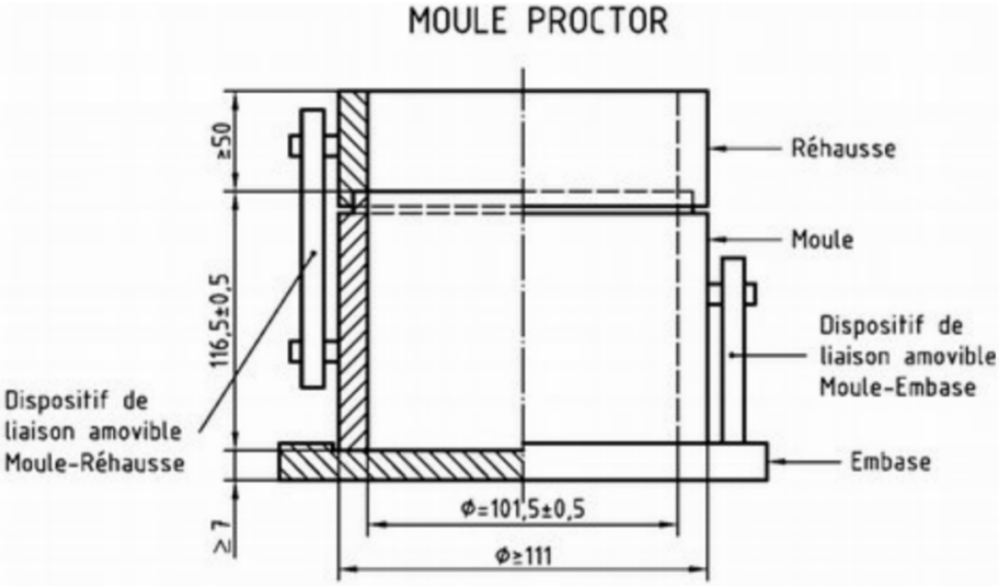


Figure B.2: CBR mould[12]

5. Divide the sample in three equal parts such that you can fill the mould in three layers. The three layers should be a bit bigger than the volume of the mould.

6. Introduce the first layer in the mould and compact it with the compaction tamper. As we are using a CBR mould, we have to drop the compaction tamper eigth times 7 drops following the pattern shown on figure B.4 , but no drop at the center during the last cycle. Repeat this step for the two other layers.

7. Remove the extension of the mould and the excess of soil with a leveling ruler. Brush the soil on the outside of the mould.

8. Weigh the mould with the soil sample in it.

9. Remove the sample from the mould and dry it to determine the real water content.

10. Repeat the method with the water contents desired.

B.3.3 Calculations

For each test we calculate:

- The water content

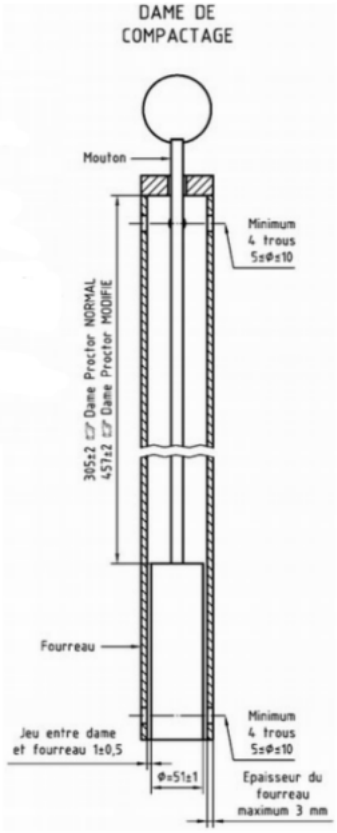


Figure B.3: Compaction Tamper [13]

- The dry mass of soil in the mould
- The dry density of the soil

The water content ω (%) is calculated using the following formula:

$$\omega = \frac{m_h - m_s}{m_s} * 100$$

Where m_h is the mass of the soil sample before drying m_s is the mass of the sample after drying in the oven.

The dry mass in the mould m_d (g) is calculated using the following formula:

$$m_d = \frac{m_w}{1 + \omega}$$

Where m_w is the wet mass of soil in the mould, calculated by substractring the mass of the mould to the total mass.

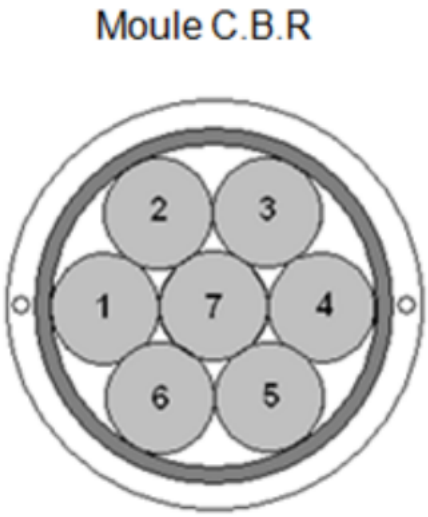


Figure B.4: Drop pattern for compaction in a CBR mould.[14]

Finally, the dry density of the soil $\rho_d(t/m^3)$ is calculated using the following formula:

$$\rho_d = \frac{\rho_w}{1+\omega}$$

Where ρ_w is the wet density of the soil.

Appendix C

Roughness graphs of the steel plate

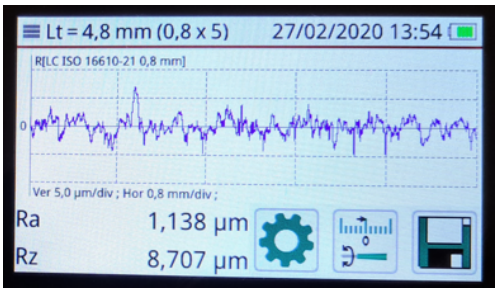


Figure C.1: First roughness test

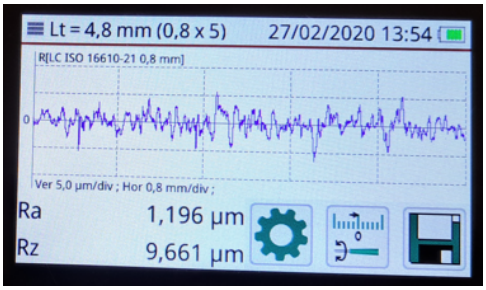


Figure C.2: Second roughness test

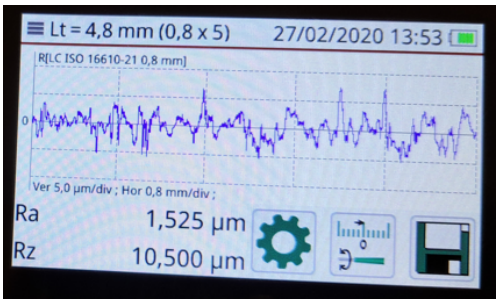


Figure C.3: Third roughness test

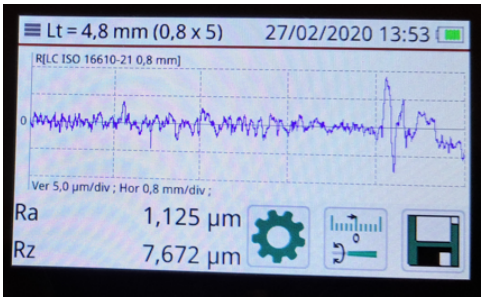


Figure C.4: Fourth roughness test

Appendix D

Assessment of axial pipe-soil resistance

D.1 Effect of soil density and normal stress

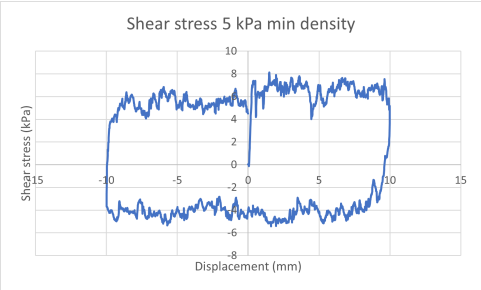


Figure D.1: Shear stress 5 kPa min density

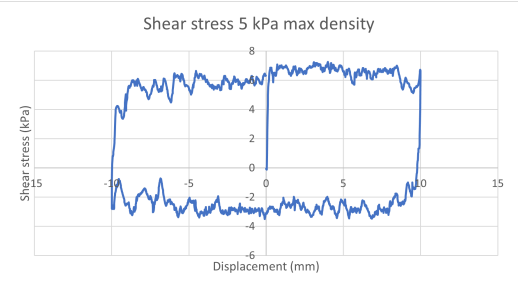


Figure D.2: Shear stress 5 kPa max density

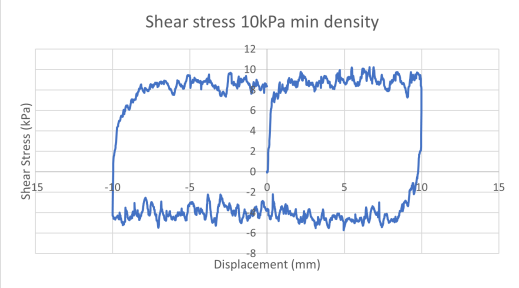


Figure D.3: Shear stress 10 kPa min density

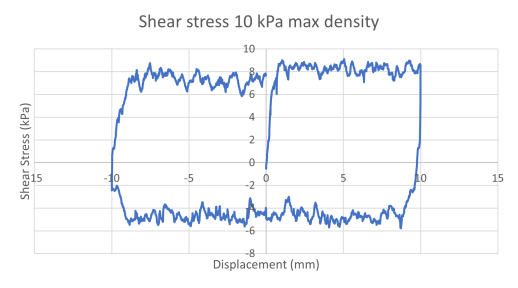


Figure D.4: Shear stress 10 kPa max density

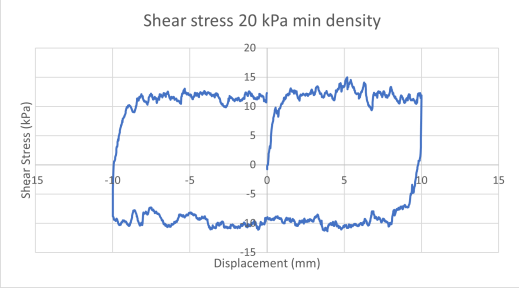


Figure D.5: Shear stress 20 kPa min density

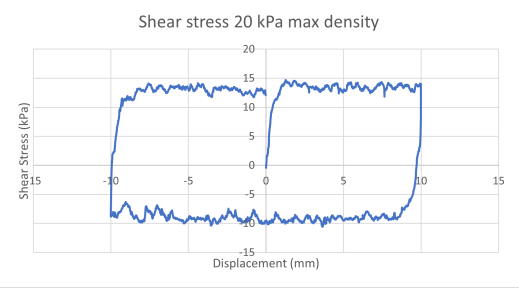


Figure D.6: Shear stress 20 kPa max density

Appendix E

Reverse direction tests

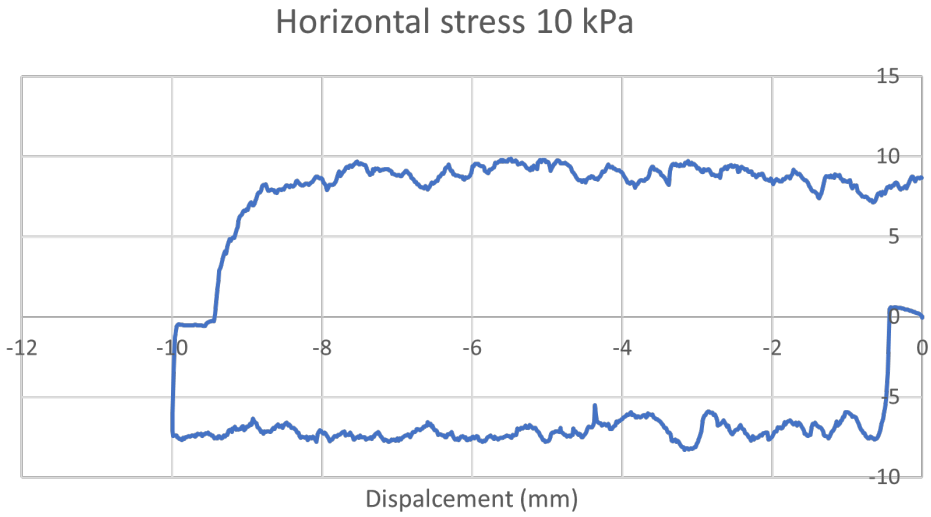


Figure E.1: Test 10 kPa reverse direction

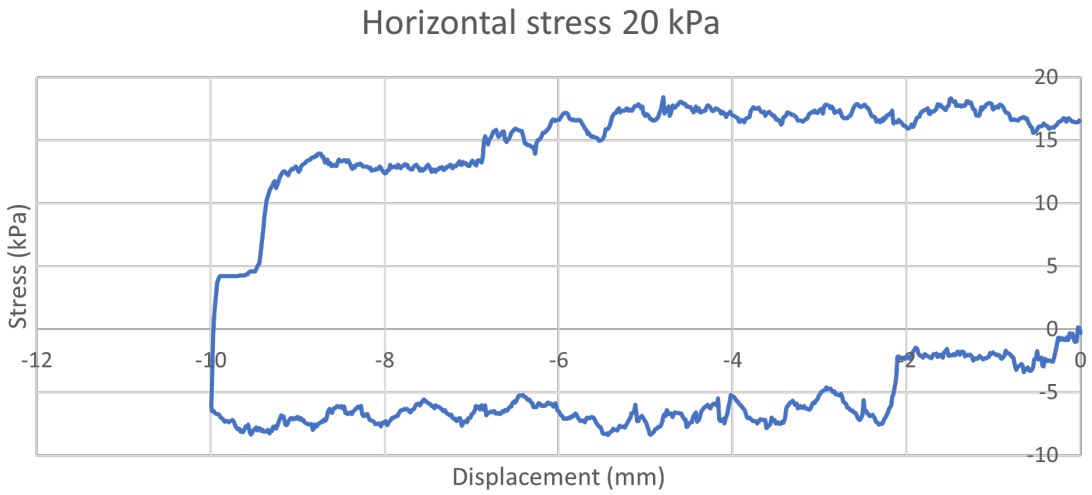


Figure E.2: Test 20 kPa reverse direction

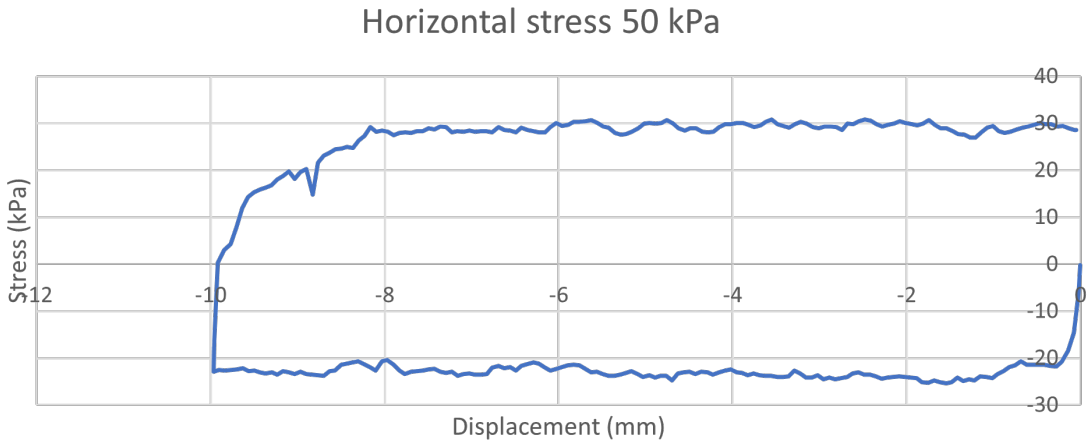


Figure E.3: Test 50 kPa reverse direction

Bibliography

[1] DJ White, EC Clukey, MF Randolph, NP Boylan, MF Bransby, A Zakeri, AJ Hill, and C Jaeck. The state of knowledge of pipe-soil interaction for on-bottom pipeline design. In *Offshore Technology Conference*. OnePetro, 2017.

[2] Nathalie Boukpeti and David J White. Interface shear box tests for assessing axial pipe–soil resistance. *Géotechnique*, 67(1):18–30, 2017.

[3] DJ White, ME Campbell, NP Boylan, and MF Bransby. A new framework for axial pipe-soil interaction, illustrated by shear box tests on carbonate soils. In *SUT Offshore Site Investigation and Geotechnics*, pages SUT–OSIG. SUT, 2012.

[4] VJ Tech. ShearSCAN Pro Motorised System. `https://www.vjtech.co.uk/LinkClick.aspx?fileticket=06xJMwHCGYY%3D&portalid\let\begingroup \escapechar\m@ne\let\MT@subst@\T1/lmr/m/it/12\def{\@@par}`, 2021.

[5] VJ Tech. VJ Tech Catalogue 10-1 Edition. urlhttps://www.vjtech.co.uk/Portals/0/Catalogue/VJ_Tech%20Catalogue_10-1_Edition.pdf.

[6] VJ Tech. An introduction to direct shear testing. `https://www.vjtech.co.uk/blog/an-introduction-to-direct-shear-testing`.

[7] VM Meyer, R Dyvik, and DJ White. Direct shear interface tests for pipe-soil interaction assessment. *Frontiers in Offshore Geotechnics III. Edited by VM Meyer*, pages 423–428, 2015.

[8] Erol Sancaktar and Rajesh Gomatam. A study on the effects of surface roughness on the strength of single lap joints. In *ASME International Mechanical Engineering Congress and Exposition*, volume 16073, pages 91–111. American Society of Mechanical Engineers, 1998.

[9] Det Norske Veritas. Dnvgl-rp-f114—pipe-soil interaction for submarine pipelines. *Det Norske Veritas*, 2017.

[10] Zack Westgate, Ricardo Argiolas, Regis Wallerand, and Jean-Christophe Ballard. Experience with interface shear box testing for pipe-soil interaction assessment on sand. In *Offshore Technology Conference*, page D011S012R004. OTC, 2021.

[11] Salahudeen Anigilaje Bunyamin, Thomas S Ijimdiya, Adrian O Eberemu, and Kolawole J Osinubi. Artificial neural networks prediction of compaction characteristics of black cotton soil stabilized with cement kiln dust. *Journal of Soft Computing in Civil Engineering*, 2(3):50–71, 2018.

[12] Benjamin Pelizzari. *Étude expérimentale des sols proches de la saturation: application aux remblais en matériaux fins*. PhD thesis, Université Grenoble Alpes, 2017.

[13] European Committee for Standardization. NF P 94-093. Sols:Reconnaissance et essais-Determination des caaractéristiques de compactactage d'un sol-Essai Proctor normal (600 $kN.m/m^3$)-Essai Proctor modifié (2700 $kN.m/m^3$). *Afnor Editions*, pages 1–17, 1993.

[14] Da Mota Paul. Fiche Technique FT 7.10.4 - L'essai Proctor. page 3, 2018.

[15] Huacan Fang and Menglan Duan. Chapter 6 - submarine pipelines and pipeline cable engineering. In Huacan Fang and Menglan Duan, editors, *Offshore Operation Facilities*, pages e1–e181. Gulf Professional Publishing, Boston, 2014.

[16] Expert market research. Global offshore oil and gas pipeline market: By diameter: Greater than 24", below 24"; by product: Oil, gas, refined products; by line type: Transport line, export line, other; regional analysis; historical market and forecast (2018-2028); market dynamics: Swot analysis; competitive landscape; industry events and developments. `https://www.expertmarketresearch.com/reports/offshore-oil-and-gas-pipeline-market-report`.

[17] Shawn Kenny. Chapter seven - offshore pipelines—elements of managing risk. In Faisal Khan and Rouzbeh Abbassi, editors, *Offshore Process Safety*, volume 2 of *Methods in Chemical Process Safety*, pages 289–325. Elsevier, 2018.

[18] Offshore Engineering. Introduction to offshore pipelines. `https://www.offshoreengineering.com/oil-gas-pipelines/1-introduction-to-offshore-pipelines/`.

[19] Aspiration energy. Why pipe sizing and flow rate is important? https://aspirationenergy.com/why-pipe-sizing-and-flow-rate-is-important/#:~:text=Optimizing%20the%20pipe%20size%20and,or%20replaced%20sooner%20than%20expected.

[20] Indovance. Piping design and modeling – importance and feasibility. https://www.indovance.com/knowledge-center/piping-design-and-modeling-importance-feasibility-2/#:~:text=Importance%20of%20Accurate%20Piping%20Design,curves%20to%20get%20processed%20quickly.

[21] DNV GL. Pipe-soil interaction for submarine pipelines. doc. no. Technical report, DNVGL-RP-F114, 2017.

[22] Paulina Dobrowolska. Shear strength using the small shear box apparatus.

[23] filament 2 print. Densities and lengths in 3d printing filaments. https://filament2print.com/gb/blog/16_densities-lengths\protect\discretionary{\char\hyphenchar\font}{}{}3D\protect\discretionary{\char\hyphenchar\font}{}{}printing\protect\discretionary{\char\hyphenchar\font}{}{}filaments.html.

[24] P NF. P 18-560: Granulats-analyse granulométrique par tamisage. *AFNOR, Paris*, 1990.

[25] Normes NF AFNOR. En 933-2 (1996),". *Essais pour déterminer les caractéristiques géométriques des granulats, Partie*, 2.

[26] MM Rahman, MA Alim, and M Shahjalal. Permeability measurement of granular materials and development of an equation. In *Proceedings of international conference on planning, architecture and civil engineering, Rajshahi University of Engineering & Technology, Bangladesh*, 2017.

[27] Ali Firat Cabalar and Nurullah Akbulut. Evaluation of actual and estimated hydraulic conductivity of sands with different gradation and shape. ncbi.nlm.nih.gov/pmc/articles/PMC4916082/#:~:text=A%20commonly%20accepted%20equation%20was,hydraulic%20conductivity%20of%20saturated%20sands.

[28] P NF. 94-059 (2000). *Sols: Reconnaissance et essais–Détermination des masses volumiques minimale et maximale des sols non cohérents*.

[29] LEADRP. A complete guide to understand surface roughness in manufacturing. https://leadrp.net/blog/a-complete-guide-to-understand-surface-roughness-in-manufacturing/.

[30] geoengineer. Direct shear test laboratory testing. https://www.geoenginee r.org/education/laboratory-testing/direct-shear-test.

[31] ZJ Westgate, DJ White, and M Savazzi. Experience with interface shear box testing for axial pipe-soil interaction assessment on soft clay. In *Offshore Technology Conference*. OnePetro, 2018.

UNIVERSITÉ CATHOLIQUE DE LOUVAIN
École polytechnique de Louvain
Rue Archimède, 1 bte L6.11.01, 1348 Louvain-la-Neuve, Belgique | **www.uclouvain.be/epl**